Marine and Petroleum Geology 176 (2025) 107346

Contents lists available at ScienceDirect

Marine and Petroleum Geology

journal homepage: www.elsevier.com/locate/marpetgeo

New method for logging identification of natural fractures in shale reservoirs: The Fengcheng formation of the Mahu Sag, China

Song Wang [a,b,*], Guiwen Wang [a,b,**], Lianbo Zeng [a,b], Peng Liu [c], Yuyue Huang [a,b], Shiqian Li [a,b], Zhishi Wang [a,b], Yuanlong Zhou [d]

[a] National Key Laboratory of Petroleum Resources and Engineering, China University of Petroleum (Beijing), Beijing, 102249, China
[b] College of Geosciences, China University of Petroleum (Beijing), Beijing, 102249, China
[c] Research Institute of Petroleum Exploration and Development, PetroChina, Beijing, 100083, China
[d] Research Institute of Exploration and Development, SINOPEC, Beijing, 100083, China

ARTICLE INFO

Keywords:
Fracture identification
Image logs
Array acoustic logs
Reservoir quality
Lacustrine shale reservoirs
Mahu Sag

ABSTRACT

Natural fractures are one of the critical types of reservoir space in lacustrine shale formations. The enrichment, preservation, and production of shale oil are closely related to these natural fractures. However, the development of various sedimentary structures in lacustrine shale can interfere with fracture identification. In this study, we combined image logging and array sonic logging methods to examine the response characteristics of natural fracture development zones in the borehole, near-wellbore, and far-wellbore regions. We integrated a new logging identification method for natural fractures and explored the relationships among mineral composition, fracture types, and reservoir quality, providing a reference for selecting sweet spots in lacustrine shale reservoirs. Core samples, thin sections, and scanning electron microscope observations of the Fengcheng Formation shale reveal characteristics of multi-scale natural fracture development. High-angle and oblique fractures, which are relatively easy to identify, were recognized using core-calibrated image logs and appear as sinusoidal features on image logs. Low-angle fractures, however, require correlation with core observations for accurate identification. Using array acoustic logging data, including shear leaky and reflected waves, we obtained radial profiles of fast and slow shear waves based on dispersion variations, enabling the determination of fracture development zones. The crossing of slowness curves of fast and slow shear waves along the radial direction and strong responses of red energy clusters in radial profiles indicate the presence of fractures. Additionally, processing of shear-wave reflected wave information remote acoustic reflection imaging profiles, allowing the identification of reflectors distant from the borehole. This resulted in a new multi-scale observation method for natural fracture identification by coupling acoustic and electrical imaging data. Applying this method, we identified natural fractures and established relationships among mineral composition, fracture types, and reservoir quality. The study indicates that high-angle and oblique fractures tend to develop in interbedded felsic shale and mudstone, while low-angle fractures are more likely to form in interbedded felsic shale, dolomitic shale, and mixed shale. Reservoir quality deteriorates with increasing clay mineral content but improves with higher felsic minerals and dolomite content. The findings of this research provide a valuable reference for improving natural fracture logging identification methods and offer guidance for achieving efficient development of lacustrine shale oil.

1. Introduction

Natural fractures are one of the important reservoir spaces in continental shale formations and play a critical role in the preservation and enrichment of lacustrine shale oil reservoirs (Anders et al., 2014). Moreover, the presence of natural fractures provides preferential pathways for artificially induced fractures and serves as an essential prerequisite for fracture selection during hydraulic fracturing (Tan et al., 2020). The existence of natural fractures can effectively enhance reservoir properties and influence the propagation and distribution patterns of artificial fracture networks, thereby exerting a decisive impact on the oil and gas quality and exploitation efficiency of shale oil

* Corresponding author. China University of Petroleum-Beijing, 18 Fuxue Road, Changping, Beijing, 102249, China.
** Corresponding author. China University of Petroleum (Beijing), China.
E-mail addresses: wangsongcupb@qq.com (S. Wang), wanggw@cup.edu.cn (G. Wang).

https://doi.org/10.1016/j.marpetgeo.2025.107346
Received 19 December 2024; Received in revised form 18 February 2025; Accepted 19 February 2025
Available online 21 February 2025

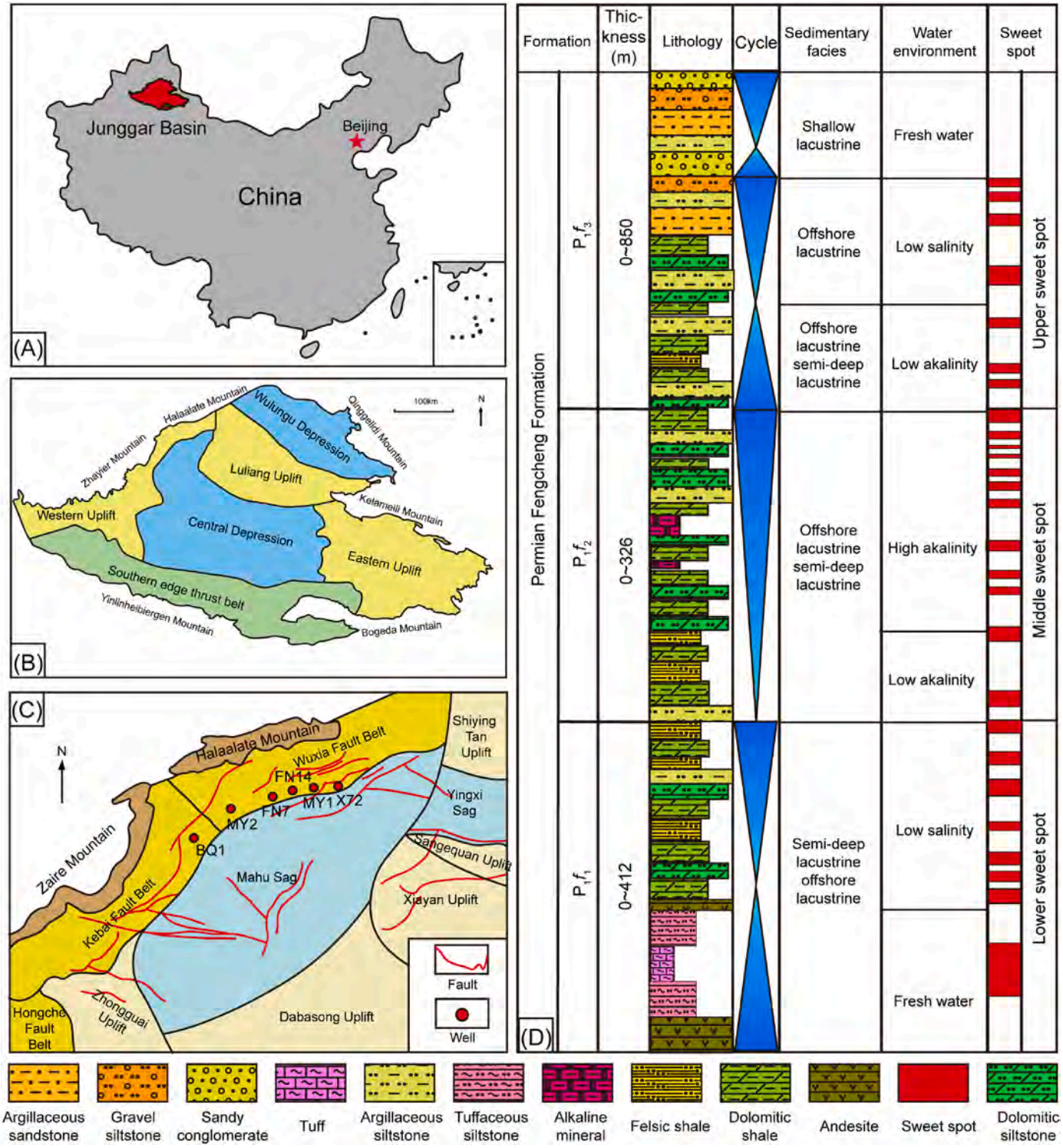

Fig. 1. (A) Location of the Junggar Basin in China. (B) Structure division of the Junggar Basin. (C) Structure division of the study area. (D) Stratigraphic column of the Fengcheng Formation in the Junggar Basin.

reservoirs (Eyinla et al., 2023; Sun et al., 2023). Therefore, studying natural fractures in lacustrine shale reservoirs is of great significance for evaluating shale oil and gas sweet spots and designing development schemes. Most continental shales in China were formed in lacustrine sedimentary environments (Huang et al., 2023; Wang et al., 2024a; Xiao et al., 2024). Due to tectonic uplift and subsidence activities, seasonal climate fluctuations, biological prosperity and decline, and alternating strong and weak material supply, lake levels experienced frequent fluctuations (Dai et al., 2021; He et al., 2024; Ma et al., 2020; Yu et al., 2021; Zou et al., 2022). The shales formed under these processes and environments often exhibit diverse mineral compositions and complex overlapping relationships of laminae, leading to uneven stress states during diagenesis and tectonic evolution (Wang et al., 2021; Xi et al., 2020; Yang et al., 2022). This exacerbates the complexity of natural fracture networks in continental shales, making the study of natural fractures in these formations particularly challenging.

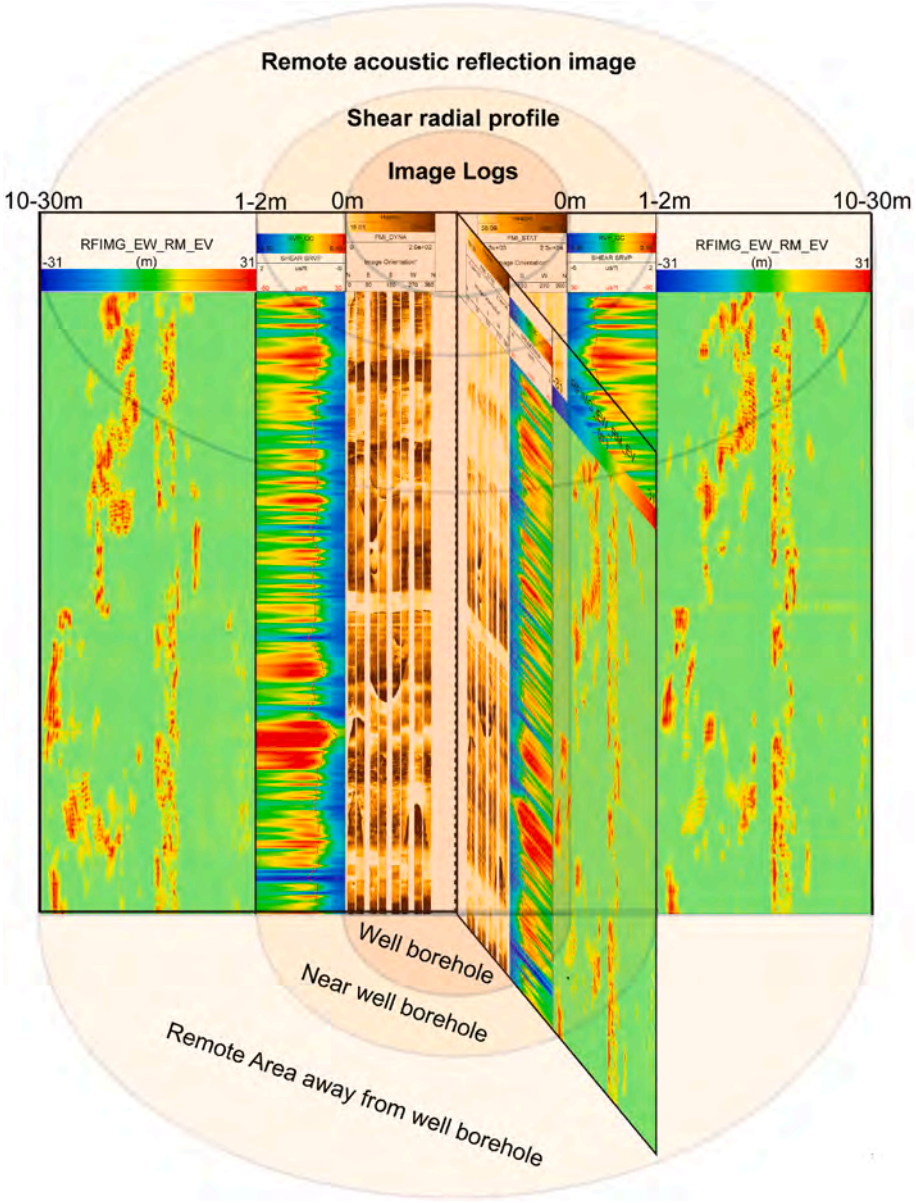

Fig. 2. Detection range and response to natural fractures of electrical image and array acoustic logging.

Over the years, scholars both domestically and internationally have focused on the development characteristics, formation mechanisms, identification methods, and distribution prediction of natural fractures, achieving significant breakthroughs in tight sandstone and carbonate reservoirs (Du et al., 2023; Guo et al., 2018; Mazdarani et al., 2023; Wang et al., 2024b; Zhang et al., 2021). In recent years, with the continuous deepening of shale oil and gas exploration and development and ongoing technological and theoretical innovations, it has been recognized that natural fractures in shale oil reservoirs exhibit obvious particularities and complexities (Zhao et al., 2020). Lacustrine shales generally possess sedimentary laminae, and structural fractures under the same stress conditions have more complex mechanical responses than those in tight sandstones or carbonates. Structural fractures tend to deviate in areas with dense sedimentary laminae, resulting in irregular fracture surfaces (Wu et al., 2024). The orientation alignment between low-angle fractures (bedding-parallel fractures) and diagenetically altered fractures formed through burial processes presents significant challenges in their differentiation using micro-resistivity imaging techniques due to their analogous spatial configurations. (Nian et al., 2021; Wang et al., 2021). In lacustrine shale reservoirs, conventional logging techniques are constrained by inadequate resolution (>1 mm), significantly impeding microfracture identification. While borehole image logs offer enhanced visualization, their diagnostic capability is frequently compromised by wellbore instability issues, compounded by the analogous geophysical responses observed among natural fractures, bedding planes, and drilling-induced fractures (Wang et al., 2021; Huang et al., 2023). The pervasive presence of fracture-filling minerals (e.g., calcite, pyrite) introduces substantial signal attenuation, effectively masking genuine fracture signatures. Furthermore, pronounced reservoir heterogeneity-manifested through erratic total organic carbon (TOC) distribution (1–8 wt%) and millimeter-scale laminations—imposes critical limitations on the quantitative assessment of fracture parameters, particularly porosity and permeability estimations (Ma et al., 2021; Lai et al., 2024). Research on multi-scale natural fracture logging identification and characterization in such reservoirs is extremely scarce, leading to insufficient understanding of the development characteristics and distribution patterns of natural fractures, which severely restricts effective exploration and efficient development of continental shale oil reservoirs. Fortunately, the development of array acoustic logging technology has brought new breakthroughs in natural fracture

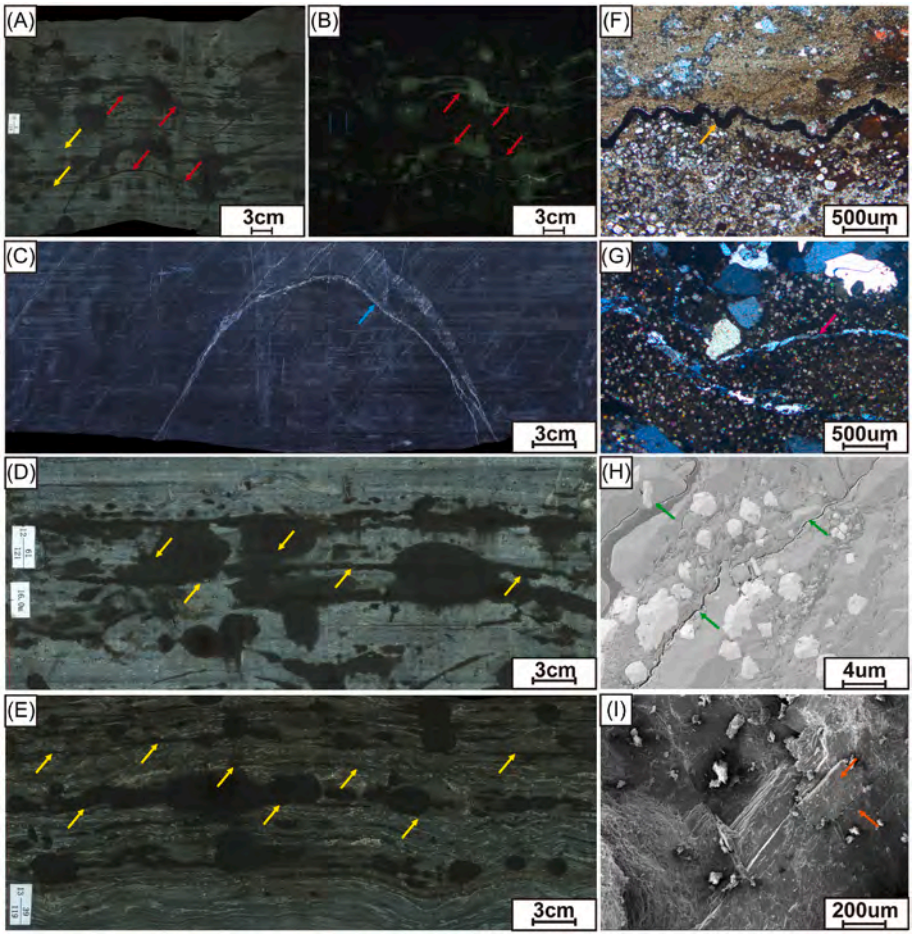

Fig. 3. Core, thin section and SEM photos show the types of natural fractures in shale rocks of the Junggar Basin. (A) Oblique fractures, MY1, 4744.27m. (B) Oblique fractures, MY1, 4744.27m, fluorescent photo. (C) high-angle fractures, FN14, 4023.81m. (D) Low-angle shear fractures with oil stain, MY1, 4729.70m. (E) Low-angle shear fractures, MY1, 4753.36m. (F) Microfractures filled with organic matter, MY1, 4674.48m. (G) Microfractures filled with hydrothermal minerals, MY1, 4709.43m. (H) Microfractures penetrating minerals, MY1, 4755.67m. (I) Microfractures penetrating dolomites, XY1, 3981.80m.

identification (Kamel and Mabrouk, 2004; Li et al., 2022; Xu et al., 2024; Zhang et al., 2024). The resolution of array acoustic logging lies between physical model experiments and fracture monitoring. By utilizing the dispersive characteristics of dipole shear waves and employing numerical simulation methods to invert the radial variation of acoustic velocity near the borehole, radial velocity profiles of dipole shear waves can be established to explore the response characteristics of natural fractures within 1–2 m around the borehole and near-wellbore area (Chen et al., 2023; Ma et al., 2021). Additionally, significant progress has been made in remote acousic reflection imaging technology, achieving a technological leap from monopole reflected P-wave profiles to dipole reflected S-wave imaging profiles. This advancement not only enables the determination of the azimuth of near-well reflectors but also extends the application range of acoustic logging to tens of meters outside the well (Zhuang et al., 2019). This development makes it possible to combine electrical imaging with array acoustic logging methods to clarify the in-situ multi-scale (borehole-near wellbore-formation) geophysical responses of natural fractures, opening up new ideas for the study of characterization methods of natural fracture distribution characteristics in lacustrine shales.

In view of this, this paper intends to investigate the responses of different types of natural fractures in image logs through core-calibrated. Subsequently, using the information of dipole shear wave leaky modes and reflected waves from array acoustic logging, we extract radial shear wave profiles and remote acousic reflection imaging profiles, explore the variation patterns of fast and slow shear waves along the radial direction, clarify the correlation between off-well reflectors and natural fractures, and verify through comparison with core and imaging results. Thus, a set of multi-scale logging identification methods for natural fractures is established. Furthermore, the relationships among natural fractures, mineral composition, and reservoir quality are explored, providing a reference for the study of the relationship between natural fractures and sweet spots in lacustrine shales, and promoting the high-quality development of lacustrine shale oil in China.

2. Geological settings

The Junggar Basin, located in the Xinjiang Uygur Autonomous Region of northwestern China, is a multi-cycle hydrocarbon-bearing basin underlain by a Carboniferous basement (Fig. 1A) (Tang et al., 2021; Zhi et al., 2021). Encircled by six major mountain ranges, the basin exhibits intense tectonic activity along its periphery while maintaining a stable central region. Based on structural deformation characteristics and geophysical properties across different areas, the basin can be further divided into six primary structural units, designated as Wulungu Depression, Luliang Uplift, Central Depression, Western Uplift, Eastern Uplift, and Southern edge thrust belt (Fig. 1B) (Cao et al., 2005). The Mahu Sag is situated on the northwestern margin of the Central depression, at the forefront of Zhayier and Halaalate mountain ranges, and connects with Wuxia and Kebai fault belts, resulting in well-developed faults and fractures (Fig. 1C) (Wang et al., 2022). From the Late Carboniferous to the Permian periods, the ocean basin

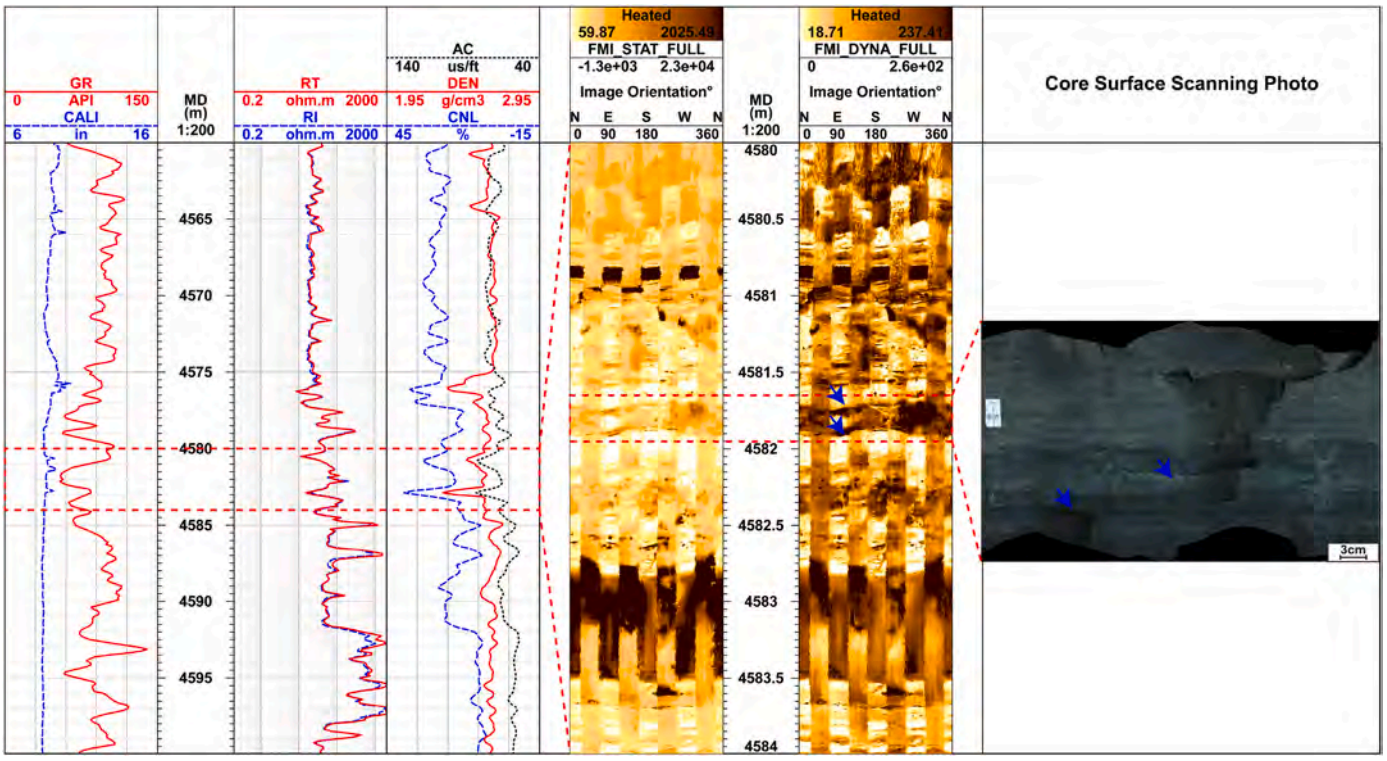

Fig. 4. Conventional and image logs response characteristics of low-angle fractures.

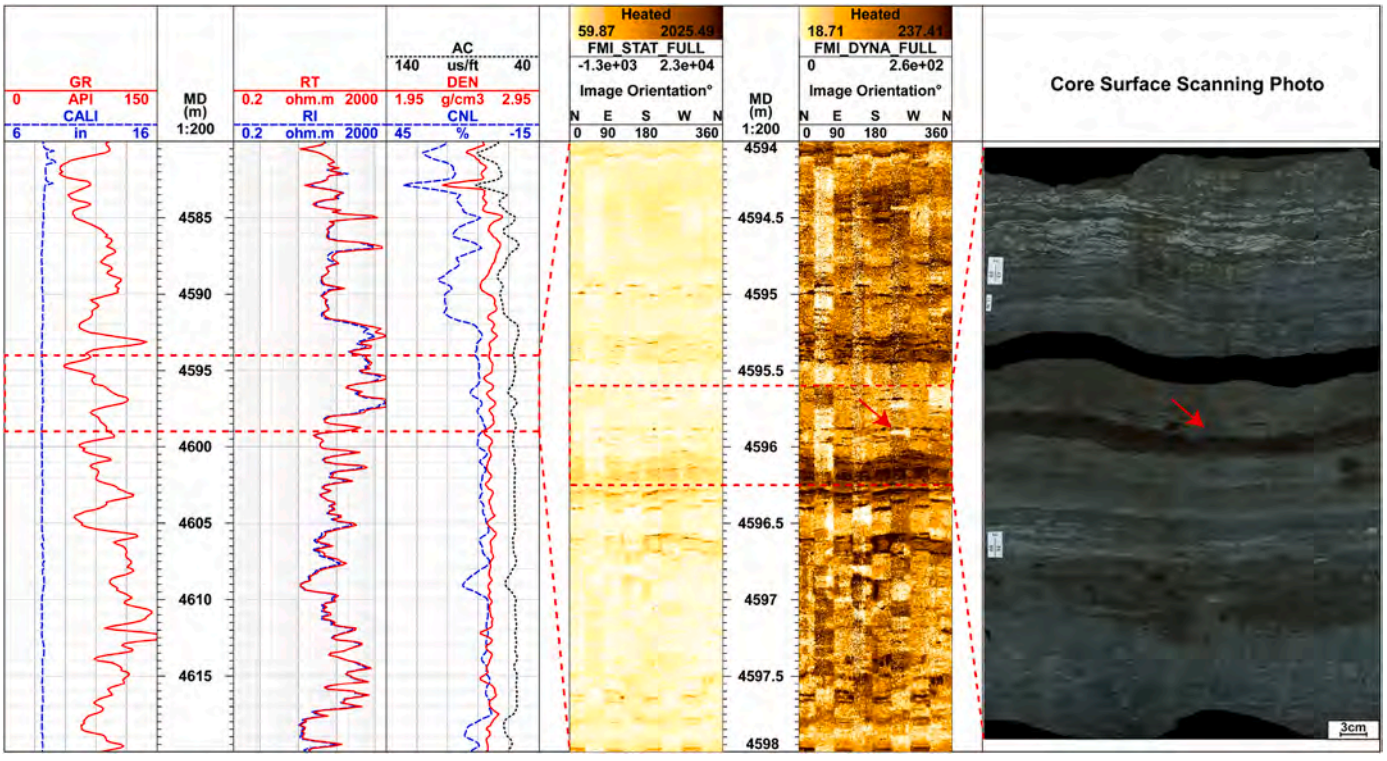

Fig. 5. Conventional and image logs response characteristics of horizontal fractures.

progressively closed from west to east. In the Early Permian, seawater retreated from multiple depressions in the western basin, leading to the formation of a relatively enclosed marginal lacustrine basin in the Central Depression (Liu et al., 2016).

The Fengcheng Formation in the Mahu Depression exhibits characteristics of a typical foreland basin structure, characterized by westward thrusting and eastward progressive overlap, with a thicker western and thinner eastern profile, and thicknesses exceeding 1800 m in the central area (Guo et al., 2021; Hu et al., 2016). Based on sedimentary cycles, lithological variations, and well-logging response

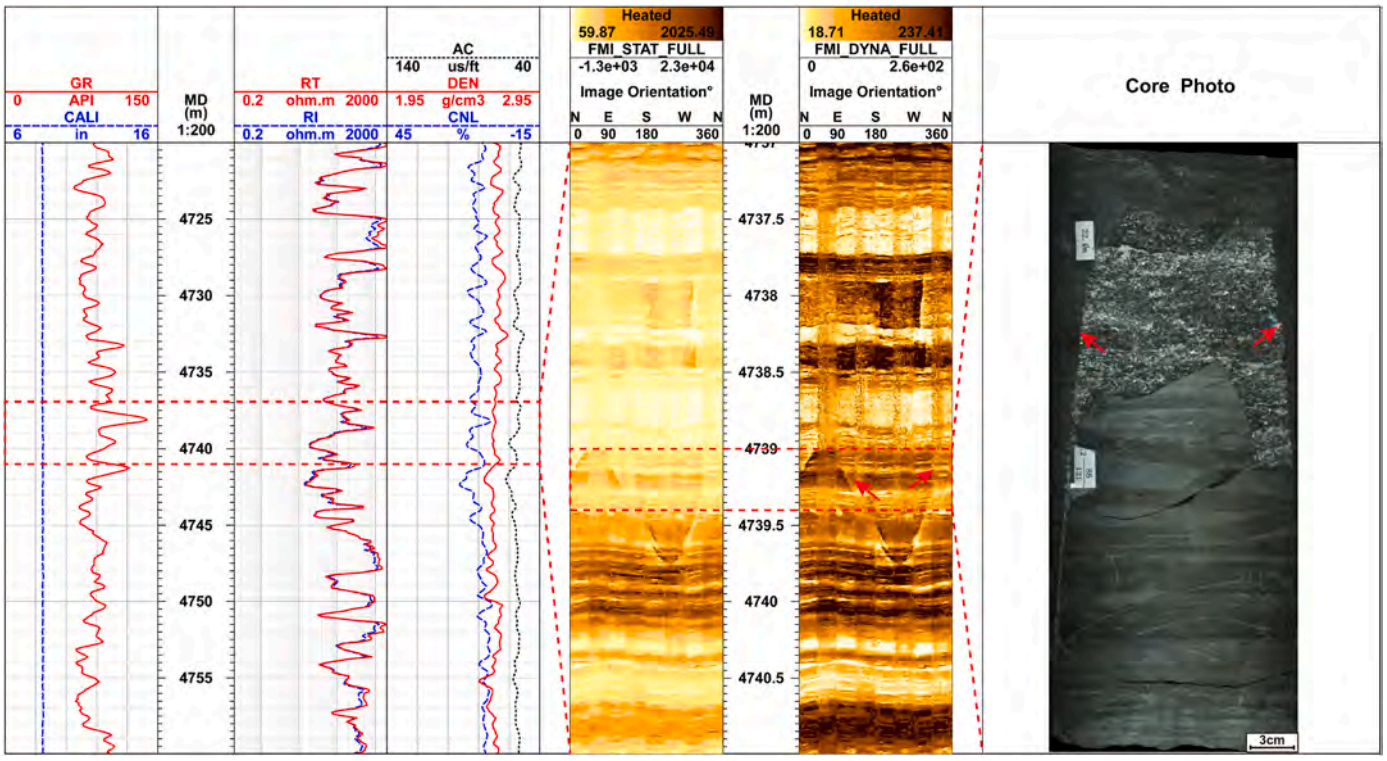

Fig. 6. Conventional and imaging logs response characteristics of high-angle filled fracture.

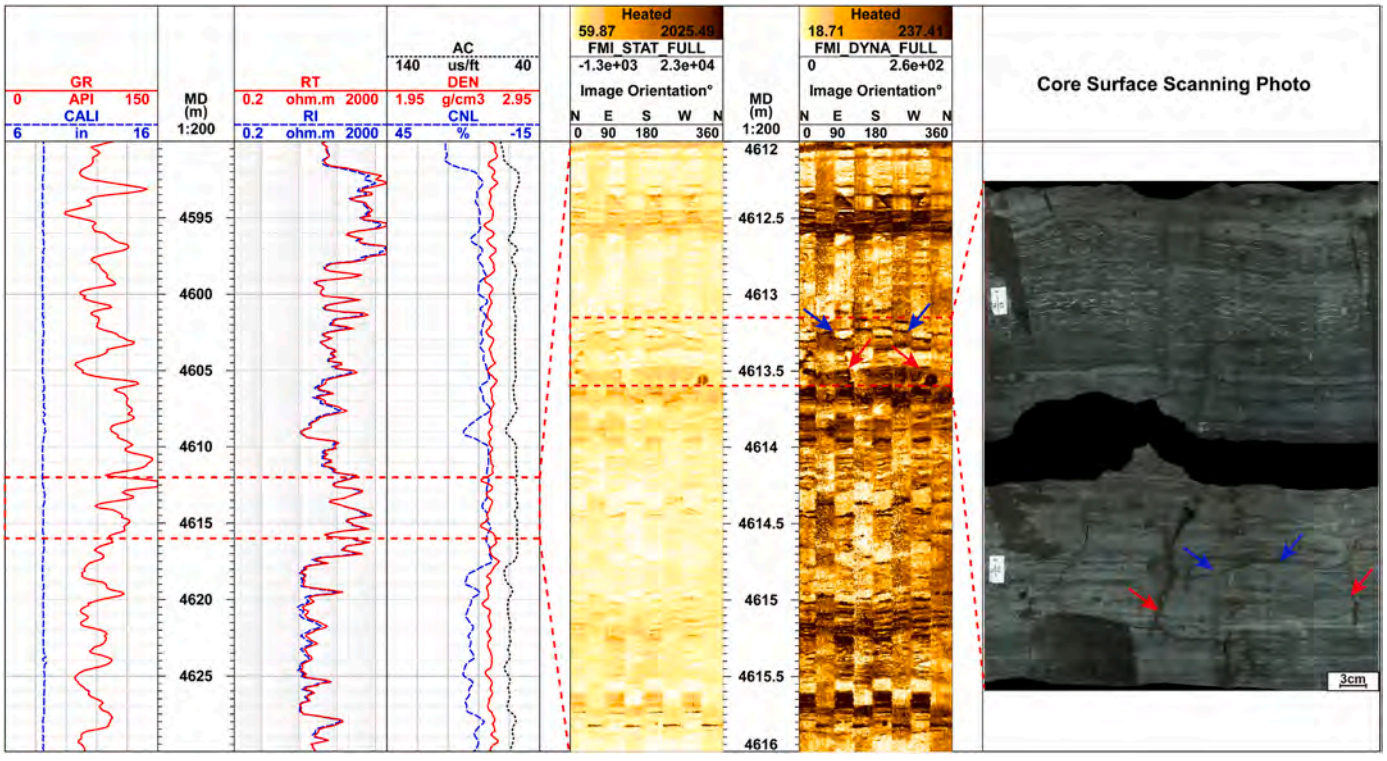

Fig. 7. Conventional and image logs response characteristics of network fractures.

characteristics, the Fengcheng Formation can be stratigraphically divided from bottom to top into three lithological members (P_1f_1, P_1f_2 and P_1f_3) (Fig. 1D) (Tang et al., 2022; Yu et al., 2018). The P_1f_1 Member was deposited in environments ranging from coastal shallow lacustrine to deep and semi-deep lacustrine settings, with volcanic clastic rocks at the base gradually transitioning upward into dolomitic siltstone and dolomitic mudstone/shale, accompanied by a slow increase in water salinity. The P_1f_2 Member was deposited in coastal shallow lacustrine to semi-deep lacustrine environments, with lithology mainly comprising dolomitic shale, felsic shale, and argillaceous siltstone, interbedded with

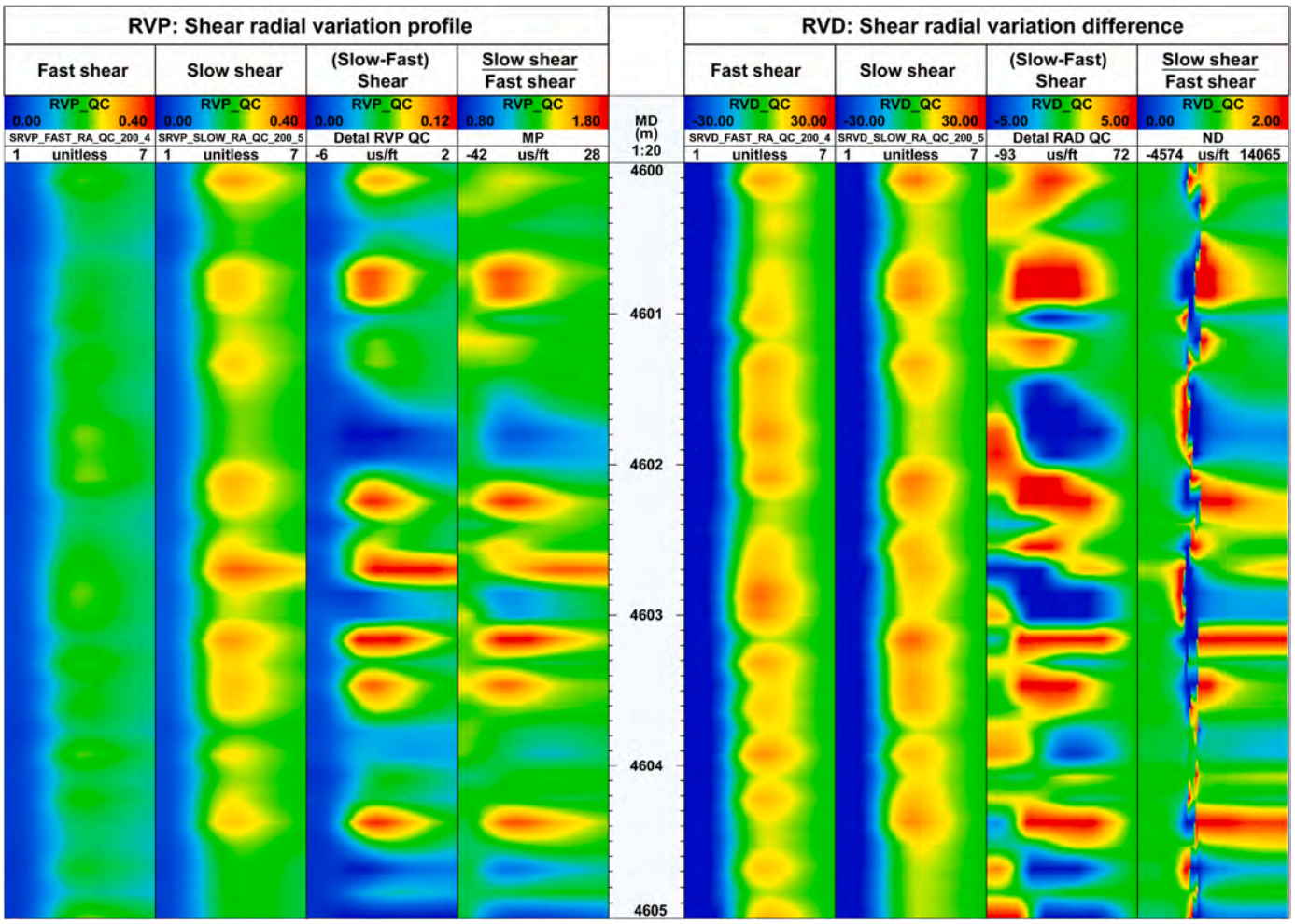

Fig. 8. The radial variation differences and profiles of the fast and slow shear waves.
RVP: radial variation differences, RVP: radial variation profiles. (Slow-Fast) = slow shear wave minus fast shear wave, (Slow/Fast) = slow shear wave divided by fast shear wave.

minor alkaline mineral layers. In the P_1f_3 Member, water salinity gradually decreased, with lithology transitioning from mudstone/shale at the base to fine sandstone and gravelly sandstone at the top, and the depositional environment evolving into shallow lacustrine and shallow lacustrine settings (Zhang et al., 2018).

3. Data and methods

Well MY1 is the only well in the study area that cored the entire well interval, obtaining a core length of 289 m in the shale section of the Fengcheng Formation. In this study, in addition to observing the physical cores, fluorescent core photographs were acquired, which not only facilitated the observation of fractures but also allowed for the assessment of their hydrocarbon-bearing potential. Furthermore, selected plug samples were ground into thin sections for microscopic examination of mineral types and microfracture characteristics. Fragment samples were also selected for further analysis of the relationships between fractures and minerals using scanning electron microscopy, thereby achieving fracture identification at the macro, meso, and micro-scales.

This study primarily explores the identification of natural fractures using logging data. Due to the varying detection ranges of different logging suites and methods, their responses to natural fractures differ accordingly (Fig. 2). Well MY1, being the only fully cored well throughout its entire interval in the study area, collected a comprehensive suite of logging data, including conventional logging, micro-resistivity imaging logging, array acoustic scanning logging, elemental scanning logging, and two-dimensional nuclear magnetic resonance (NMR) logging. The conventional logging data encompass caliper, gamma ray, deep and shallow resistivity, compressional slowness, neutron porosity and density curves. In this study, micro-resistivity image logs was performed using Schlumberger's Formation Micro-Imager (FMI) instrument. Beyond standard procedures such as acceleration correction, pad equalization correction, dynamic and static image generation, and shallow resistivity-calibrated static image, the gaps between the pads were filled, increasing pad coverage to 100%. This enhancement effectively reduces the ambiguity in identifying borehole fractures to a certain extent (Brekke and Roenitz, 2021; Khoshbakht et al., 2012). The study primarily utilizes leaky and reflected wave information from sonic scanner (Li, 2023). By conducting dispersion inversion to obtain radial profiles of fast and slow shear waves, we established a response relationship between the radial differences of these shear waves and natural fractures, thereby identifying fractures within a 1–2 m range around the borehole (Zhang et al., 2024). Since reflected waves propagate over longer distances, they can be processed using seismic data processing methods such as filtering, stacking, and migration to invert the acoustic logging reflected wave information into images analogous to seismic profiles, enabling the identification of faults distant from the borehole (Wang et al., 2020). This method develops a multi-scale fracture identification methodology that combines electrical imaging for borehole fracture identification, shear radial variation

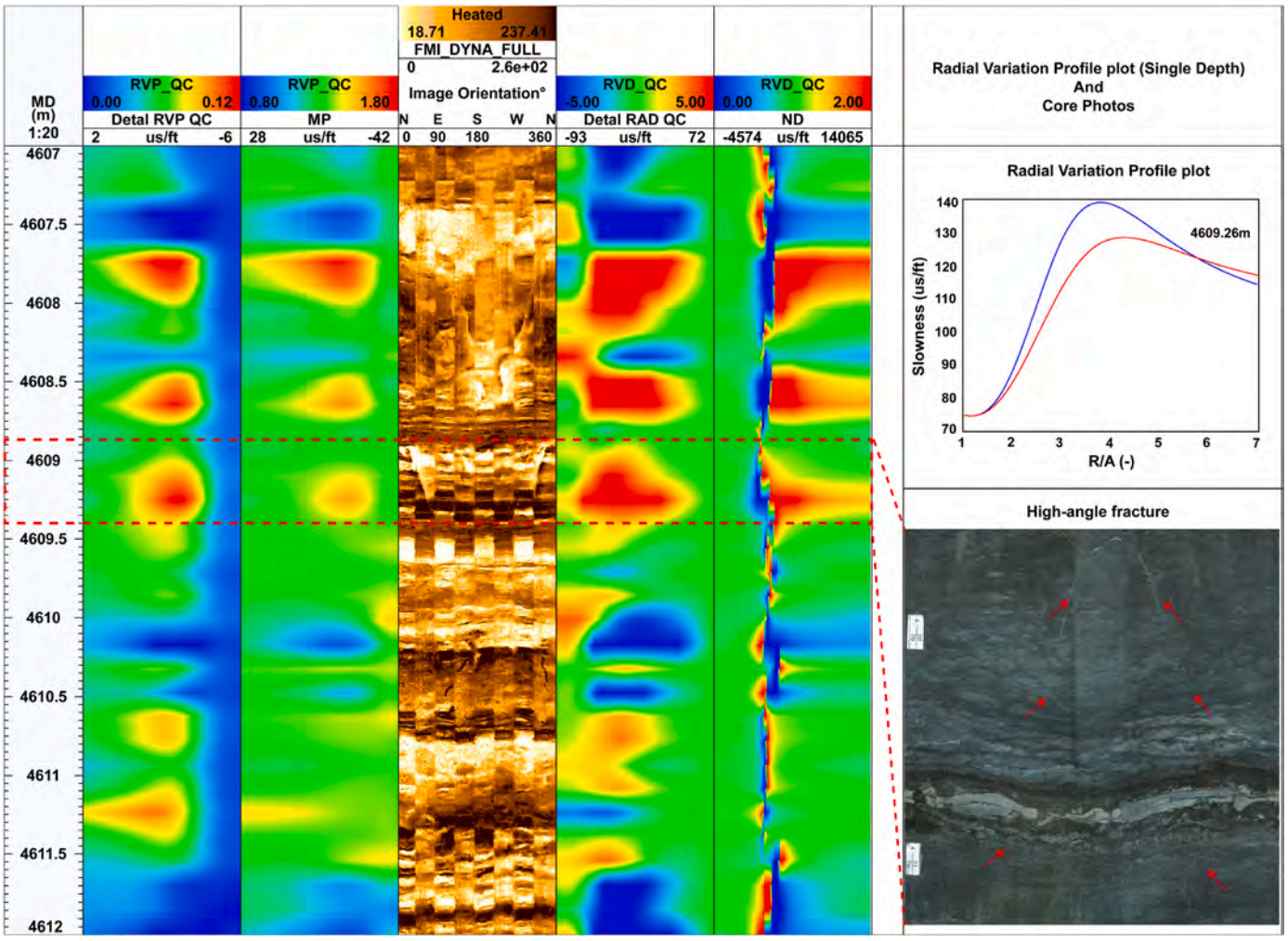

Fig. 9. The shear variation and image log response characteristics of high-angle natural fracture.

profile for detecting fractures outside the borehole, and remote acoustic reflection image for recognizing reflectors in regions further from the wellbore. This integrated approach effectively reduces the ambiguity associated with fracture identification when relying on a single method.

4. Results

4.1. Reservoir fractures characteristics

Fractures are not only significant reservoir spaces but also key factors in enhancing reservoir permeability and lowering the thresholds of reservoir physical properties. Observations from cores, thin sections, and scanning electron microscopy (SEM) reveal that the natural fractures in the Fengcheng Formation of the Mahu Sag exhibit multi-scale characteristics. These include centimeter-scale fractures observable in cores, millimeter-scale fractures visible under an optical microscope, and micro-to nano-scale fractures identifiable under SEM. Fractures observed in cores allow for the determination of fracture dip angles and filling characteristics, such as oblique fractures (Fig. 3A and B), high-angle fractures (Fig. 3C), and low-angle fractures (Fig. 3D and E). These fractures predominantly develop in thin-layered felsic shale and laminated dolomitic shale. In the fluorescence photomicrographs, sinusoidal yellow fluorescence is clearly observed along the fracture surfaces (Fig. 3B). Additionally, oil stains developed along these fracture surfaces are evident in Fig. 2D, indicating a close association between the fractures and oil-bearing properties. An increased number and density of shale laminae promote the development of bedding fractures and low-angle fractures. Both high-angle and low-angle fractures exhibit features of mineral filling and organic matter filling (Du et al., 2023). Microscopic fractures provide clearer observations of filling types and crystal forms. Organic matter often appears as dark, irregular linear distributions along fractures (Fig. 3F). Hydrothermal mineral fillings are observed as pure, large crystals under cross-polarized light (Fig. 3G). SEM observations reveal fracture characteristics of different brittle minerals, with some microfractures even cutting through mineral grains (Fig. 3H and I).

4.2. Well log responses characteristics in fractrues of the shale reservoirs

4.2.1. The image logs response

Micro-resistivity image logging is currently the highest-resolution method for identifying natural fractures using logging data (Khoshbakht et al., 2012; Wang et al., 2021). The response characteristics of natural fractures in shale reservoirs differ significantly from those in conventional sandstone reservoirs and fracture-vuggy carbonate reservoirs. In conventional sandstone and carbonate reservoirs, mud invasion leads to a noticeable resistivity contrast between the reservoir matrix and the fracture surfaces. Compared to shale reservoirs, these conventional reservoirs exhibit less pronounced stratification, making it easier to observe complete sinusoids in image logs (Ju et al., 2020; Lai et al., 2024). In contrast, shale reservoirs display strong vertical heterogeneity in both composition and structure. Variations in mineral composition or depositional structures can cause subtle, layered alternations of light and dark in image logs, increasing the difficulty of

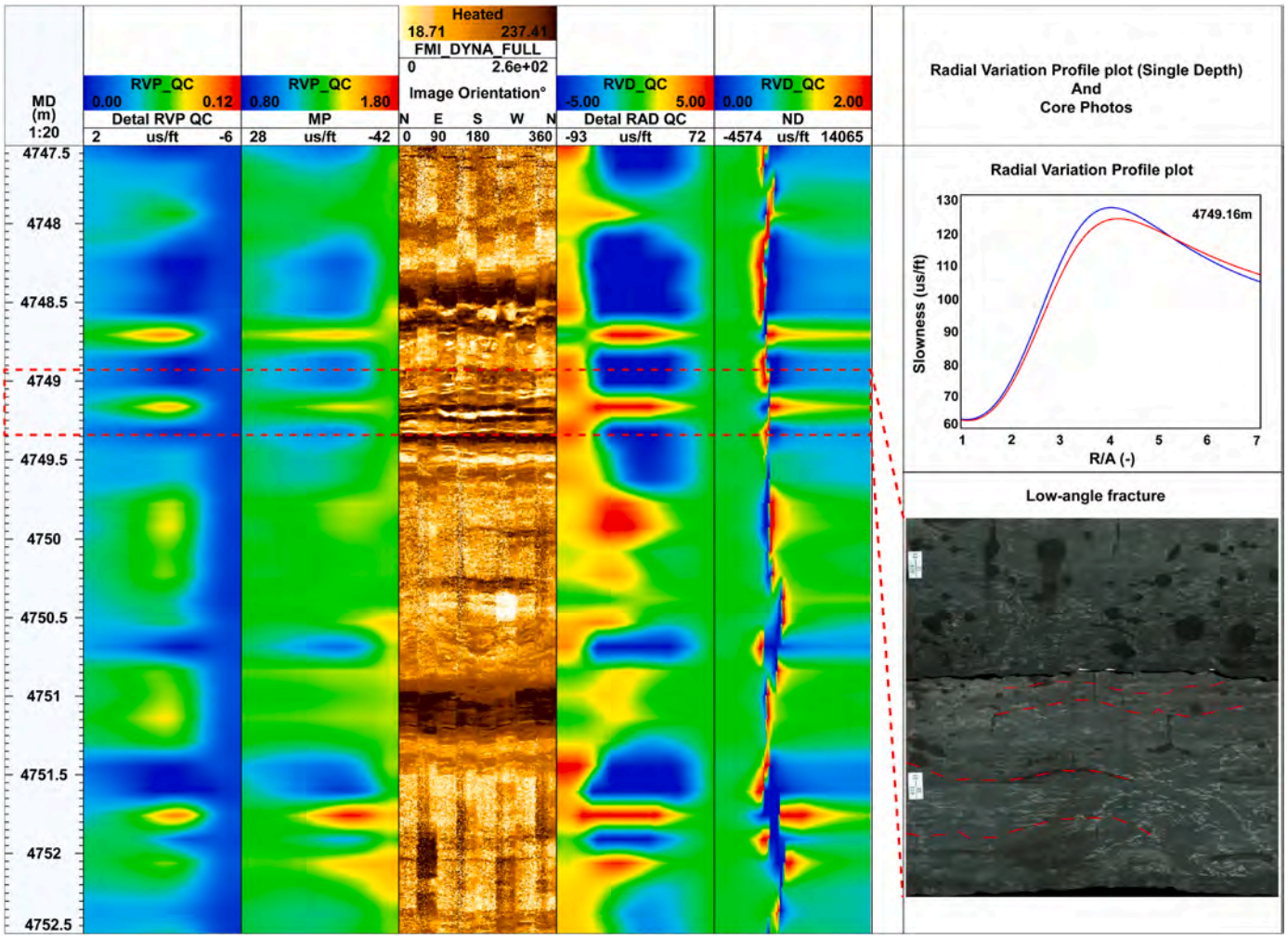

Fig. 10. The shear variation and image log response characteristics of low-angle natural fracture.

identifying low-angle fractures and horizontal fractures.

By comparing conventional logs, imaging logs, and core photographs, identification chats were established (Figs. 4–7). Figs. 4 and 5 illustrate the response characteristics of low-angle fractures and horizontal fractures, respectively. On image logs, low-angle, partially filled fractures appear as indistinct, dark sinusoidal lines, while conventional logs show minimal differentiation between deep and shallow resistivity readings (Fig. 4). Horizontal fractures exhibit strong similarities to shale bedding in image logs, the primary distinction is that horizontal fractures appear as intermittent sinusoidal lines with uneven thickness, reflecting irregular bituminous infilling or variations in fracture aperture within a single fracture (Fig. 5). Simultaneously, conventional logs display positive differences between deep and shallow resistivity. However, even with these responses, it is insufficient to conclusively identify fractures as bedding fractures without corroboration from core samples and additional data. High-angle fractures are easier to identify than low-angle fractures due to their significant differences in texture and orientation compared to shale reservoirs. Fig. 6 depicts high-angle fractures: conventional logs exhibit sharp resistivity peaks, image logs show distinct bright-edged sinusoidal lines, and core samples reveal obvious calcite mineral fillings. During core examination, hydrochloric acid titration results in the emergence of numerous fine bubbles from the fracture surfaces. While such fractures in zones with good matrix reservoir properties do not enhance permeability, they become critical factors for fracture initiation during hydraulic fracturing layer selection. Fig. 7 displays a network of fractures partially filled with oil and gas. Conventional logs indicate increased resistivity, image logs show only portions of sinusoidal lines without peaks or troughs, and the core samples are relatively fragmented with good oil saturation. This represents the most favorable scenario in reservoir evaluation. When coupled with siltstone bands possessing excellent matrix properties, these conditions constitute the highest-quality reservoirs.

4.2.2. *The shear radial variation profile response*

The most significant application of traditional monopole acoustic logging in reservoir evaluation is calculating porosity and identifying gas layers using compressional slowness (P-wave). In contrast, array acoustic logging employs dipole sources, which can excite shear waves (S-waves). Shear waves undergo dispersion during propagation and split into fast and slow shear waves in anisotropic formations (Mazdarani et al., 2023; Trichandi et al., 2023). Because shear wave dispersion is related to propagation distance, and the distances between the source and the various receivers in array acoustic logging differ, it becomes possible to invert radial slowness using the dispersion characteristics of fast and slow shear slowness (Nian et al., 2021). In this study, we utilized the slowness of fast and slow shear obtained from dispersion inversion to process the shear radial variation profiles and differences. This approach amplifies the response of radial acoustic differences to natural fractures. Specifically, operations on the radial profiles and differences of the fast and slow shear waves included calculating the difference (slow shear wave minus fast shear wave) and the ratio (slow shear wave divided by fast shear wave), thereby enhancing the signals associated with formation anisotropy (Fig. 8). By comparing these results with core images, we can determine the radial responses of fractures. Additionally, variations

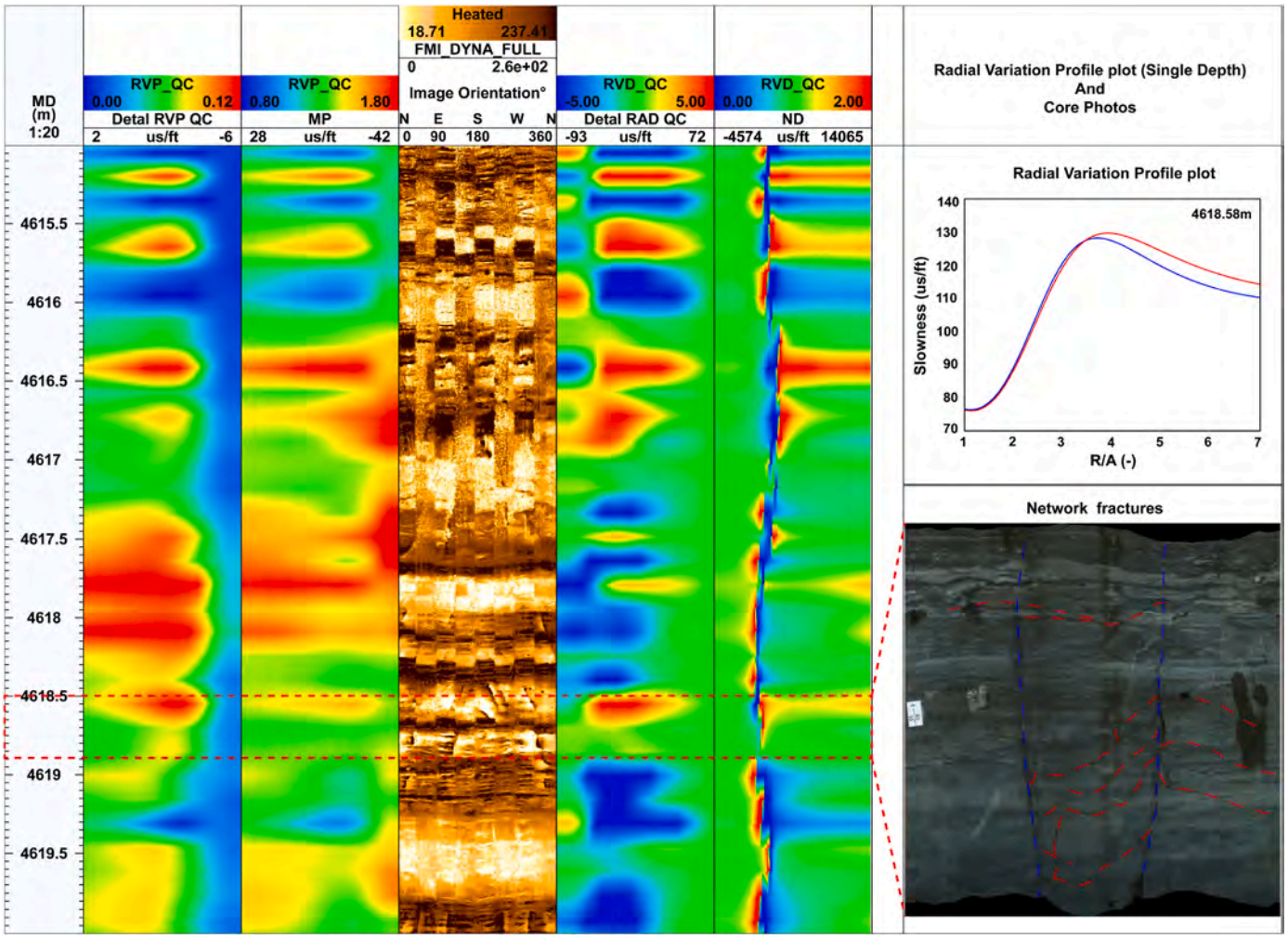

Fig. 11. The shear variation and image log response characteristics of network natural fracture.

in the radial transit times of fast and slow shear waves and their crossover points are used to verify the presence of natural fractures.

Figs. 9–11 illustrate the radial profiles of shear wave differences in fracture-developed zones, dynamic full-coverage electrode electrical imaging, and crossplots comparing radial distance with fast and slow shear wave time differences from logging responses. This analysis establishes the correlation between shear wave response characteristics within a radial range of 1–2 m and the matching relationships among imaging logs and core fractures. In Fig. 9, the interval from 4608.8 m to 4609.4 m represents a typical fracture-developed section. Tracks 2, 3, 5, and 6 display intensely strong red energy clusters, indicative of positive differential responses where the slow shear slowness exceeds that of the fast shear wave. We extracted the radial variation of the fast shear slowness at 4609.26 m and observed that both the fast and slow shear slowness initially increase and then decrease. Notably, there is an intersection point where the fast and slow shear slowness are equal, indicating significant heterogeneity within the reservoir. The electrical image logs at the corresponding depth exhibits a large-amplitude sinusoidal trace, and the corresponding core photo reveals a high-angle natural fracture.

Due to the extremely dense lamination in shale formations, the orientations of horizontal fractures, sedimentary laminae, and bedding planes are nearly identical. This results in similar image logs responses, making them difficult to distinguish. However, shear waves in the radial direction exhibit distinct response characteristics. Fig. 10 presents the radial shear wave and electrical imaging logging responses of low-angle fractures. Similar to the red acoustic energy clusters observed for high-angle fractures in Fig. 9, red acoustic energy cluster responses also appear here. However, these acoustic energy clusters appear compressed, forming linear responses, which indicates that the fractures do not extend widely in the vertical direction. The image logs display a horizontal layered pattern representing the orientations of fractures, while core photo reveal groups of low-angle fractures. At a depth of 4749.16 m, the slowness responses of fast and slow shear waves during radial propagation similarly increase and then decrease, with an intersection point appearing. This behavior indicates the presence of fractures. Therefore, by integrating the responses of acoustic energy clusters with image logs, it is possible to distinguish between sedimentary laminae and low-angle fractures.

Fig. 11 illustrates the logging responses within a mesh-like fracture zone formed by the interaction of low-angle and high-angle fractures. In the depth interval from 4618.5 m to 4618.9 m, imaging logs exhibit both high-angle sinusoidal curves and dark laminar responses, indicating the presence of multiple fracture types. Core images also reveal various fractures. Due to the abundance of horizontal laminae, the acoustic energy clusters display an elliptical shape, and the four red energy clusters show significant morphological differences. At a depth of 4618.58 m, the radial time difference between fast and slow shear waves initially increases and then decreases. When the parameter R/A (gradient) exceeds 4, the time difference of the fast shear wave becomes greater than that of the slow shear wave, indicating a reversal phenomenon between the fast and slow shear wave time differences. Regardless of whether the fractures are high-angle, low-angle, or mesh-like, positive differential responses appear in the radial acoustic energy

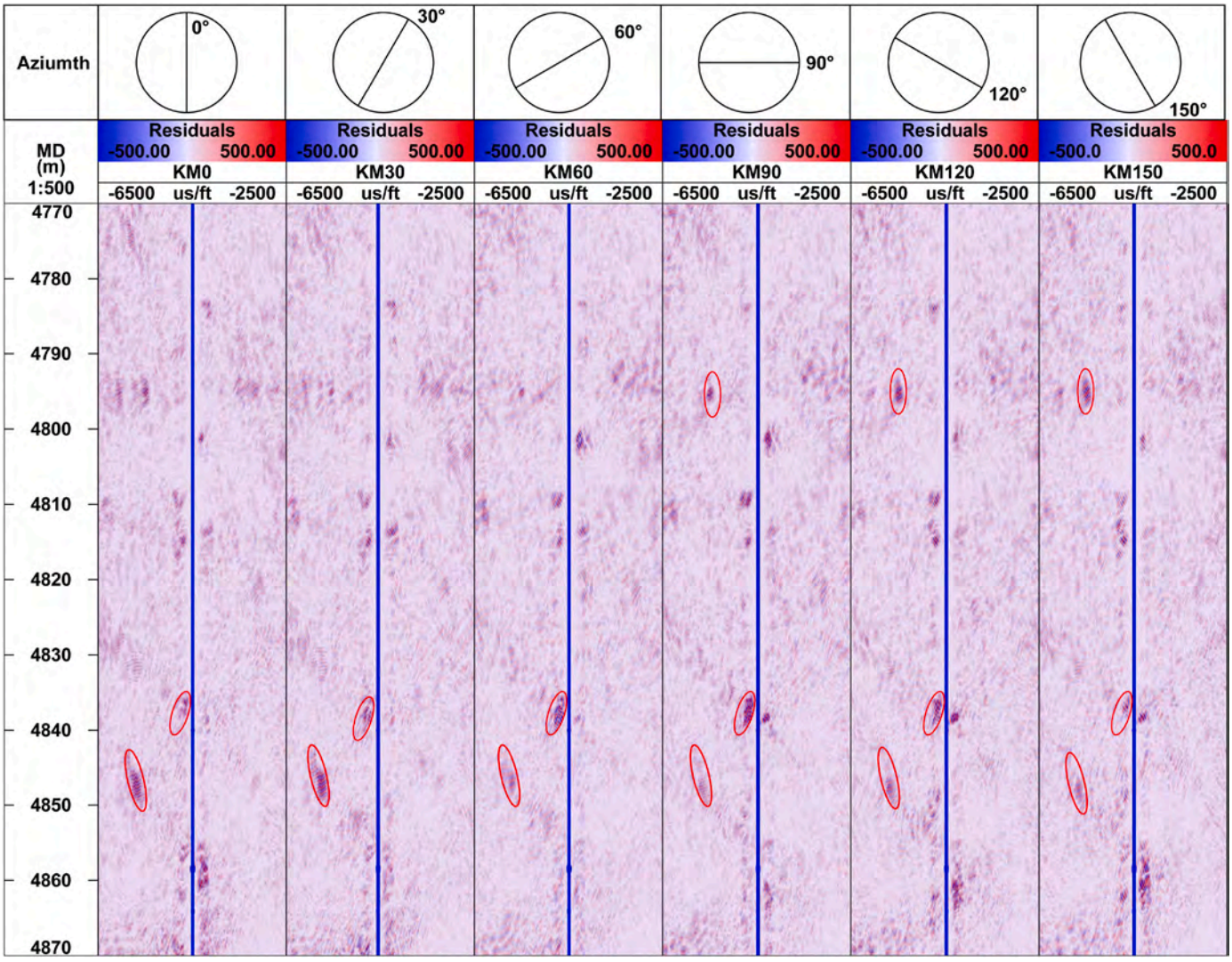

Fig. 12. The remote acoustic (shear) reflection imaging response at various azimuths of Well MY1.

clusters, manifested as red energy clusters that correspond well with fractures observed in core samples. Because the detection range of acoustic logs extends farther than that of borehole image, these acoustic responses can serve as a bridge between far-field detection and borehole detection in the evaluation of fracture systems.

4.2.3. The remote acoustic reflection imaging response

The remote acoustic logging technique, also known as reflection acoustic logging, enables the detection and evaluation of geological anomaly reflectors, such as fractures, cavities, and faults-within tens of meters outside the borehole (Wang et al., 2020; Wu et al., 2020). This significantly extends the application scope of acoustic logging technologies. Typically, acoustic logging instruments generate high-frequency acoustic signals within the borehole ranging from 1 to 20 kHz (Kamel and Mabrouk, 2004). The acoustic energy primarily propagates along the borehole wall, producing refracted compressional and shear waves, as well as Stoneley waves. By increasing the radiated power of the acoustic source, more energy penetrates the borehole wall and enters deeper into the formation (Li et al., 2022). When this energy encounters geological structures with acoustic impedance contrasts relative to the surrounding formation, such as fractures, cavities, or reservoir boundaries, it is reflected back to the borehole in the form of reflected waves, which are recorded by receiving transducers (Fu et al., 2024; Xu et al., 2024). By extracting these reflected waves from the recorded data and performing migration imaging, parameters such as the position, orientation, and morphology of reflectors outside the borehole can be determined. Actual measurements have demonstrated that the radial detection range of remote acoustic logging can cover distances from 3 to 50 m, with a resolution of approximately 1 m, greatly expanding the detection capabilities of logging technology.

In this study, we employed sonic data collected using Schlumberger's Sonic Scanner instrument to extract shear-wave reflection profiles at various azimuths, specifically at 0°, 30°, 60°, 90°, 120°, and 150° (Fig. 12). The reflectors observed in these profiles exhibit energy of varying intensities, with the strongest energy indicating the azimuth corresponding to the strike direction of the reflector. At a depth of 4850 m, the reflector shows the strongest energy in the due north and north-northeast directions, while at 4840 m, the strongest energy is observed in the east-west direction. By analyzing these energy variations, we determined the azimuth and strike of the reflectors. Furthermore, combining this information with the spatial relationship between the reflectors and the borehole wall allowed us to ascertain the apparent dip of the reflectors. Fractures are only one component of fault systems. In previous studies, fractures associated with boreholes have predominantly been identified using electrical imaging. However, due to the complexity of fracture morphology and spatial extension, relying solely on electrical imaging logging can lead to ambiguous interpretations in the identification of natural fractures. Therefore, to accurately identify

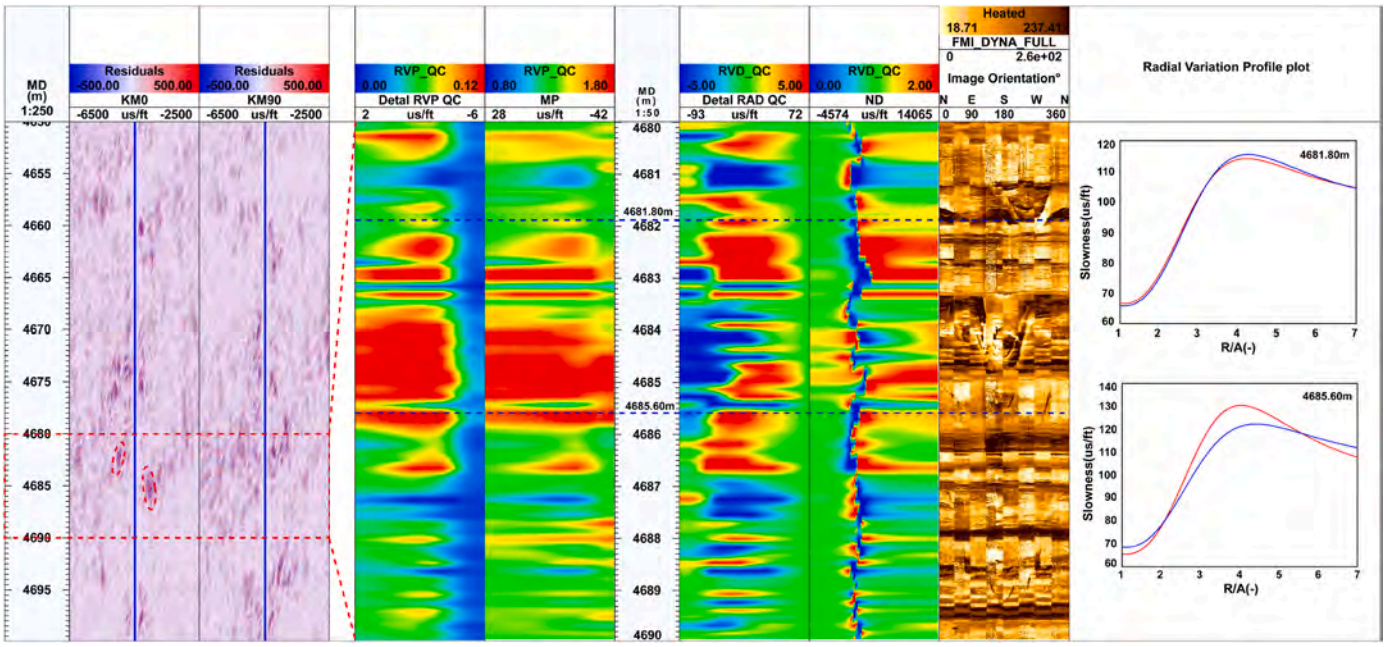

Fig. 13. Multiscale response characteristics of remote acoustic, shear variation profiles and image logging integrated methods in fractures.

natural fractures, it is necessary to integrate remote acoustic reflection image, the red energy clusters observed in the radial profiles of shear waves, and the radial variations of fast and slow shear-wave slowness.

5. Discussion

5.1. Multi-scale well logging identification of natural fractures

Fig. 13 presents the far-field remote acoustic reflection images in a fault-developed interval, the radial differential energy clusters of shear waves, dynamic electrical image logs, and the radial variations of fast and slow shear waves at specific depth points. Among these, the remote acoustic reflection images represent logging responses at the formation scale distant from the borehole (large scale), the radial profiles of shear waves and travel-time variations represent near-borehole circumferential logging responses (medium scale), and the dynamic electrical image logs represent logging responses at the well borehole (small scale). In Fig. 13, the interval between 4650 m and 4700 m in well MY1 is highlighted, with the 4680–4685 m section exhibiting the most prominent reflection characteristics. Reflectors are observed in both the north-south and east-west azimuthal profiles; however, the reflectors in the north-south direction are more concentrated (indicated by red elliptical dashed lines), while those in the east-west direction are more dispersed, exhibiting chaotic reflection features. Upon further scaling down, significant radial differences between fast and slow shear waves are observed within the 4682–4686 m range, appearing as extensive areas of red energy clusters. Correspondingly, the image logs reveal multiple sets of sinusoidal traces with notable differences in amplitude and azimuth. This indicates that natural fractures are well-developed in this interval with inconsistent orientations, representing a typical network fracture. At specific depth points of 4681.80 m and 4685.60 m, crossover points of fast and slow shear waves along radial propagation are evident in the radial gradient intersection plots. Notably, at 4685.60 m, two crossover points are observed, demonstrating extremely strong heterogeneous propagation characteristics. In summary, by integrating the multi-scale response characteristics of different logging methods at the same depths, it is evident that natural fractures definitively exist within this reservoir interval. Therefore, the natural fracture identification method established in this study—based on the combined use of acoustic and image logging data, not only enhances the accuracy of identifying natural fractures compared to solely using image logs data but also expands the applicability of logging data in natural fracture identification.

5.2. Distribution of fractures in a single well

By integrating constraints from remote acoustic reflection image, radial shear-wave energy clusters, and image logging response characteristics, natural fractures in the shale interval of key well MY1 were identified, resulting in a total of 239 fractures being cataloged (Fig. 14). Based on dip angles, these fractures were classified into three types: low-angle fractures (dip angle <30°), oblique fractures (dip angle between 30° and 60°), and high-angle fractures (dip angle >60°). Specifically, 141 low-angle fractures were identified, with fracture strikes predominantly trending north-northeast. The dip angles ranged from 1.5° to 26°, with an average of 5.35°, exhibiting a strong correlation with the bedding planes (azimuth between 50° and 60°, northeast direction, average dip angle of 5.15°). A total of 28 oblique fractures were observed, mainly trending southeast (aziumth 140°–150°), oblique fractures in other orientations were also present, with an average dip angle of 45.75°. Additionally, 70 high-angle fractures were identified, primarily trending southwest (aziumth 230°–240°) and near-south (azimuth 160°–170°), with an average dip angle of 75.84°. In general, high-angle and oblique fractures are the result of tectonic stress, while low-angle fractures are controlled by the combined effects of diagenesis and tectonic stress. The variations in fracture orientations among the different dip-angle classifications reflect the complexity of the fracture system in the Fengcheng Formation shales of the Mahu Sag.

Well MY1 also acquired elemental scanning logs (Litho scanner) to analyze the mineral composition of the shale intervals. Logging calculations indicated that the main mineral constituents of the Fengcheng Formation in the Mahu Sag are clay, quartz, potassium feldspar, sodium feldspar, calcite, and dolomite, along with minor amounts of pyrite (Zhu et al., 2018). The vertical distribution of mineral assemblages can be divided into three sections, corresponding to different types of natural fractures (Fig. 15). The upper section primarily consists of interbedded felsic shale and mixed shale. Static image reveals alternating dark bands and bright massive interlayers, displaying an overall stratified appearance. The dominant types of natural fractures in this section are high-angle fractures and oblique fractures, with fewer occurrences of low-angle fractures. The middle section is characterized by higher clay

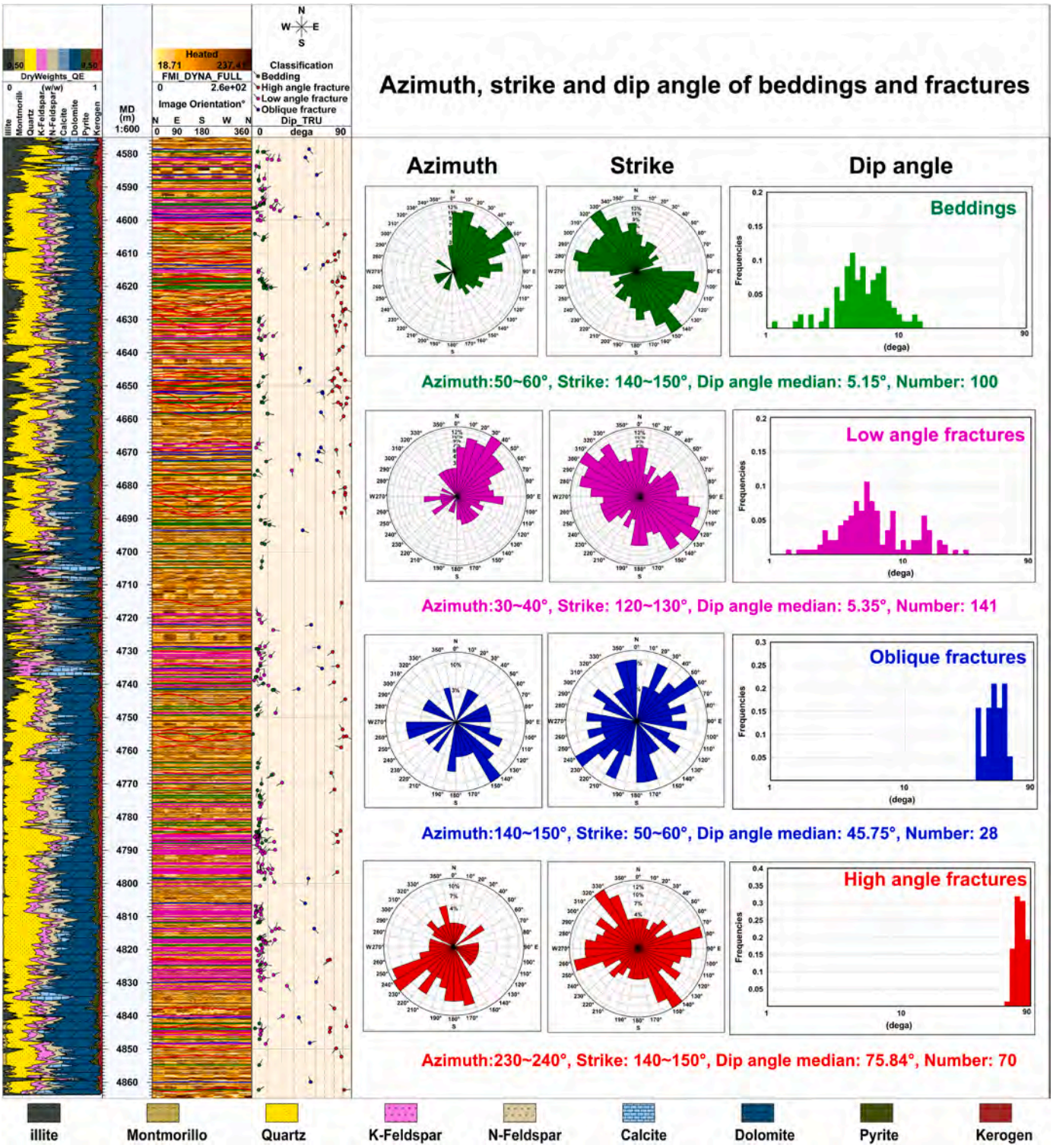

Fig. 14. Distribution of fractures and its attitude Parameters in a single well.

content, with rock types mainly comprising argillaceous mudstone and mixed shale, interbedded with small amounts of calcareous shale. This section exhibits a low number and density of natural fractures. The lower section consists mainly of felsic shale and dolomitic shale, image logs show bright massive features. The natural fractures in this section are predominantly low-angle fractures, followed by high-angle and oblique fractures.

Core observations reveal that the felsic shale of the Fengcheng Formation in the Mahu Sag contains abundant centimeter-thick feldspathic sand layers. These rocks readily form high-angle and oblique natural fractures under stress. In the dolomitic shale, dolomite primarily exists in the form of millimeter-scale laminae (Fig. 3E), the lamination interfaces act as planes of weakness under stress. Consequently, these rocks are more prone to forming low-angle fractures that are consistent with the lamination orientation and exhibit low dispersion under the combined effects of diagenesis and tectonic stress. Due to the relatively high content of plastic minerals in mixed shale, its ability to form natural fractures under tectonic stress is limited.

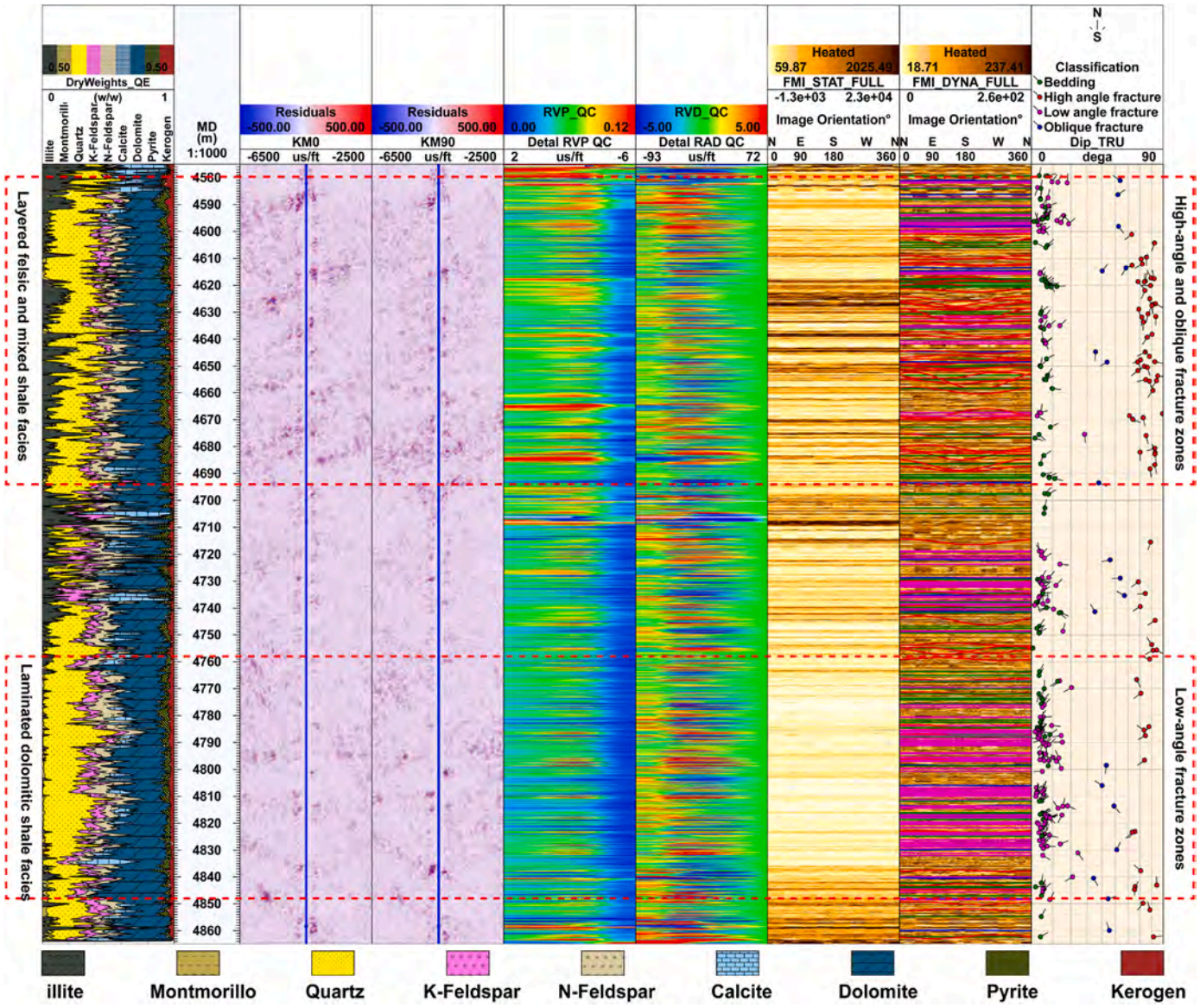

Fig. 15. The relationship between lithological assemblage and types of natural fractures.

5.3. *The relationship between fractures and reservoir quality*

Due to the inherent correlation between lithofacies assemblages and the occurrence of natural fractures, layereded felsic shales interbedded with clay-rich mudstones are associated with network and high-angle fractures, whereas laminated dolomitic mud-shales interbedded with felsic shales correspond to low-angle fractures. Therefore, this study discusses the coupling relationship between fractures and reservoir quality by segmenting based on lithofacies assemblage types. Specifically, utilizing mineral profiles calculated from elemental logging (Lithoscanner) and comparing the natural fractures identified by our method with the response characteristics of two-dimensional nuclear magnetic resonance (CMR-NG) logging energy clusters (Cai et al., 2024; Fleury and Romero-Sarmiento, 2016; Zhu et al., 2018), we explore the relationships among mineral composition, natural fractures, and reservoir quality.

Nuclear magnetic resonance (NMR) logging was selected for its ability to continuously provide T_1 and T_2 information, which is used to analyze reservoir pore structures and fluid types. The T_1-T_2 crossplot for this purpose was proposed and promoted by Schlumberger in 2015 (Fig. 16A). However, there are two unavoidable issues when using the crossplot in practice. First, when T_2 is very large, the T_1/T_2 ratio loses its significance, leading to errors in identification results. Second, the measurement signals are derived from North American shale formations, and because shale reservoirs differ across regions and stratigraphic intervals, calibration is required before use. In this study, a comprehensive analytical approach was employed to produce a T_1-T_2 crossplot for identifying pore structures and fluid types. Initially, single-point T_1-T_2 crossplots were constructed using inversion results of T_1 and T_2, where red clusters represent areas with relatively high T1 and T_2 peak values. By comparing these results with fluid production types at perforation locations and referencing classical crossplots, the final crossplot was established (Fig. 16B). Clusters 1, 2, 3, 5, 6, 8, and 9 are concentrated in the lower-left corner of the crossplot and are classified as bound water. Cluster 4 is identified as bitumen (T_2 peak <10 ms, and T_1 peak close to 100 ms). Clusters 6, 9, 11, and 13 lie along the $T_1 = T_2$ diagonal, commonly referred to as the water line, and are defined as water. Portions exceeding the cutoff value are classified as movable water. Cluster 7 exhibits a relatively high T_1 value, but its corresponding T_2 peak does not exceed the cutoff value, and $T_1/T_2 > 10$, thus it is classified as bound oil (immovable oil). Clusters 10, 12, and 14 are located in regions corresponding to movable fluids with T_2 values

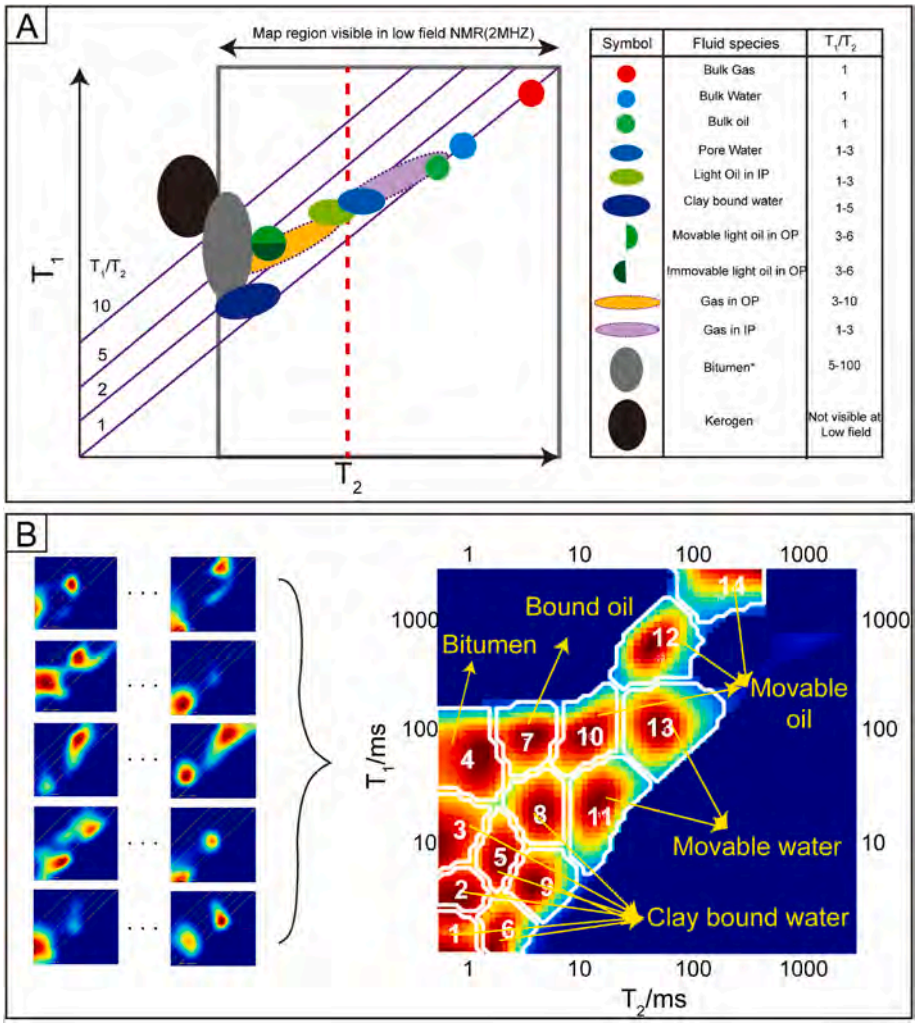

Fig. 16. Fluid type identification chart based on two-dimensional nuclear magnetic resonance logging. (A) T1-T2 identify pore and fluid type cross-plot (Modified by Kausik et al., 2016); (B) Fluid type identification chart according to 2D NMR logs (MY1).

exceeding the cutoff value. Their T_1 values are also almost entirely greater than 100 ms, and T_1/T_2 values are generally above 10, thereby classifying them as movable oil.

In the depth interval of 4645–4660 m, the lithology is predominantly felsic shale interbedded with mudstone, where network fractures are developed (Fig. 17). We examined the influence of variations in clay mineral content on reservoir effectiveness. First, we selected two points with relatively high clay mineral content (4649.81 m and 4650.00 m) and plotted two-dimensional NMR T_1-T_2 correlation maps. The images displayed double energy cluster characteristics, revealing a lower-left cluster (both T_1 and T_2 not exceeding 10 ms) representing clay-bound water, and a middle cluster (both T_1 and T_2 exceeding 10 ms) indicating potential fluids. Subsequently, we plotted two points with lower clay mineral content and higher felsic content (4652.99 m and 4656.79 m). The two-dimensional NMR energy clusters still exhibited double-cluster features. However, the area and intensity of the cluster representing bound water were smaller than those in the mudstone interval. The right-side cluster had a T_1/T_2 ratio of 10, and the portion representing free fluids demonstrated excellent oil-bearing properties (e.g., at 4656.79 m). In the interval of 4680–4690 m, the lithology mainly consists of felsic shale interbedded with mixed shales, and the clay mineral content is lower than that in the 4645–4660 m interval. High-angle fractures are predominantly developed here. We first selected depths corresponding to mixed shales (4681.83 m and 4686.30 m) and plotted two-dimensional NMR correlation maps. Two energy clusters appeared, and compared to the mudstone interval, the lower-left cluster overall shifted to the right, indicating a relatively lower content of clay-bound water. The right-side cluster exhibited signals of movable oil, with T_1/T_2 ratios of 3 at 4681.83 m and 10 at 4686.30 m. We then plotted two-dimensional NMR correlation maps in the felsic shale interval, where three energy clusters were observed. The interval at 4682.15 m exhibited the best physical properties but showed responses of bound oil, movable water, and movable oil. Although a bound water cluster appeared in the lower-left corner at 4683.10 m, two movable oil signals were present on the right side.

The intervals of 4785–4787.5 m and 4809–4811.5 m are characterized by low clay mineral content and high felsic content, with the rock type being felsic shale (Fig. 18). The two-dimensional NMR energy clusters displayed features entirely different from those of shale intervals with higher clay mineral content. At depths of 4786.40 m and 4810.68 m, the right-side energy clusters were prominent and exhibited characteristics of movable oil. At 4787.53 m, the left-side cluster presented a strong asphaltene response, while at 4810.48 m, small amounts of asphaltene, bound water, and movable mixed fluid characteristics were observed. The 4820–4830 m interval is a section with low clay mineral content and relatively high dolomite content, classified as dolomitic shale. The corresponding two-dimensional NMR energy clusters displayed multi-cluster responses, representing complex pore structures and fluid types, including bound water, movable water, movable oil, and a small amount of asphaltene. This complexity arises

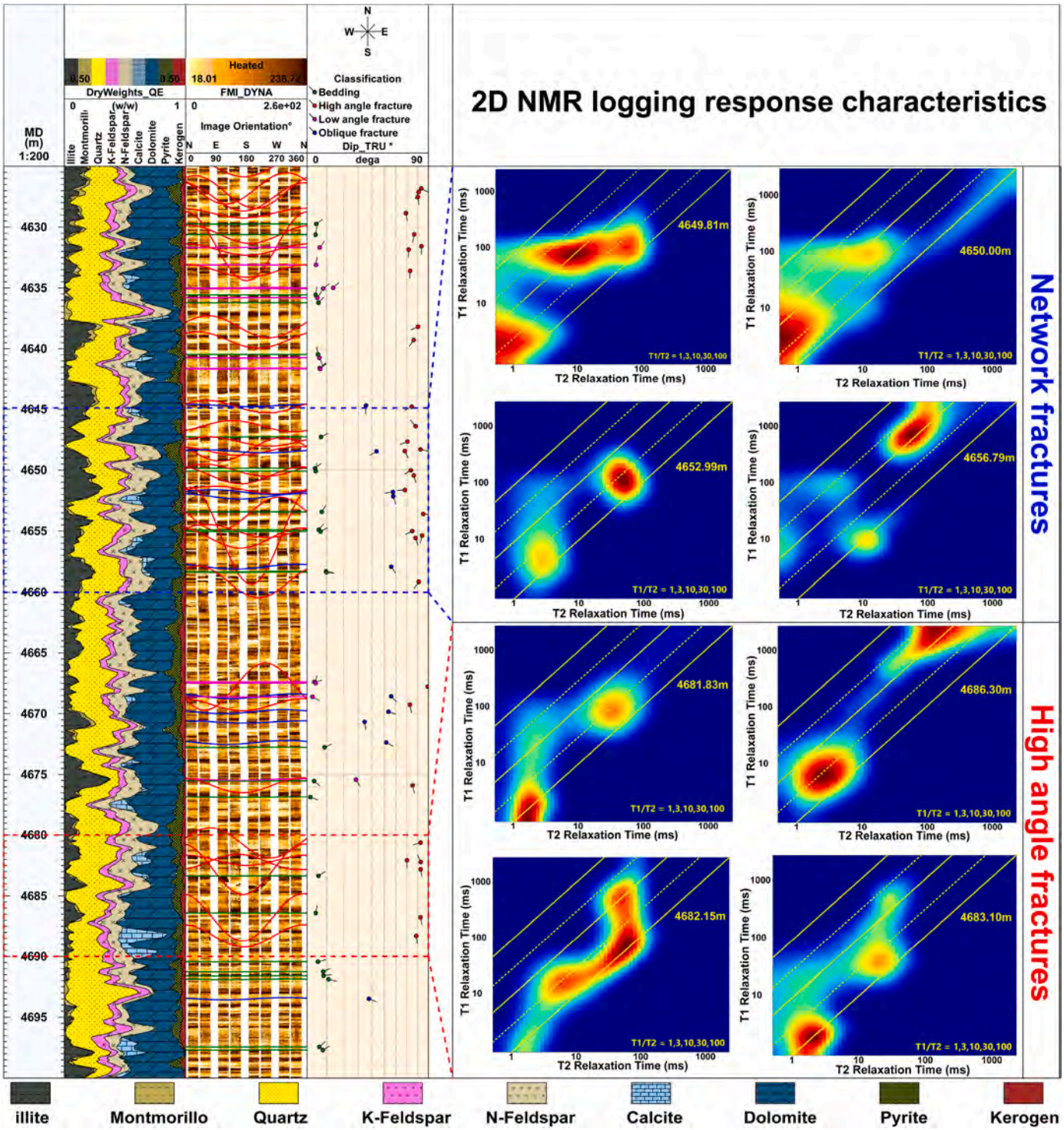

Fig. 17. The relationship between reservoir quality and natural fractures in the lithofacies assemblage unit of interbedded felsic shale and mudstone.

because the felsic content in this interval is not low, and the pore types mainly include intergranular pores among felsic mineral particles, intercrystalline pores within dolomitic laminae, and bedding fractures. The diverse reservoir space types result in complex pore structures, leading to fluid diversity within the reservoir.

In summary, higher clay mineral content corresponds to poorer reservoir quality, with fluids predominantly comprising bound water. Conversely, higher felsic content indicates better reservoir quality, with fluids mainly consisting of movable oil. When formations comprise interlayers of felsic shale and clayey mudstone, they exhibit strong heterogeneity. Rocks under tectonic stress are more likely to develop complex fracture networks, and high-angle fractures readily form in intervals with relatively high felsic content. Therefore, hydraulic fracturing to enhance production should focus on layers with higher contents of brittle minerals (felsic minerals and dolomite) and lower clay mineral content. This approach not only ensures that the fluid type is movable oil but also facilitates the formation of more complex fracture networks under the influence of primary high-angle fractures. In intervals with low clay mineral content, rocks are mainly composed of brittle minerals, and lamination and foliation are well-developed in

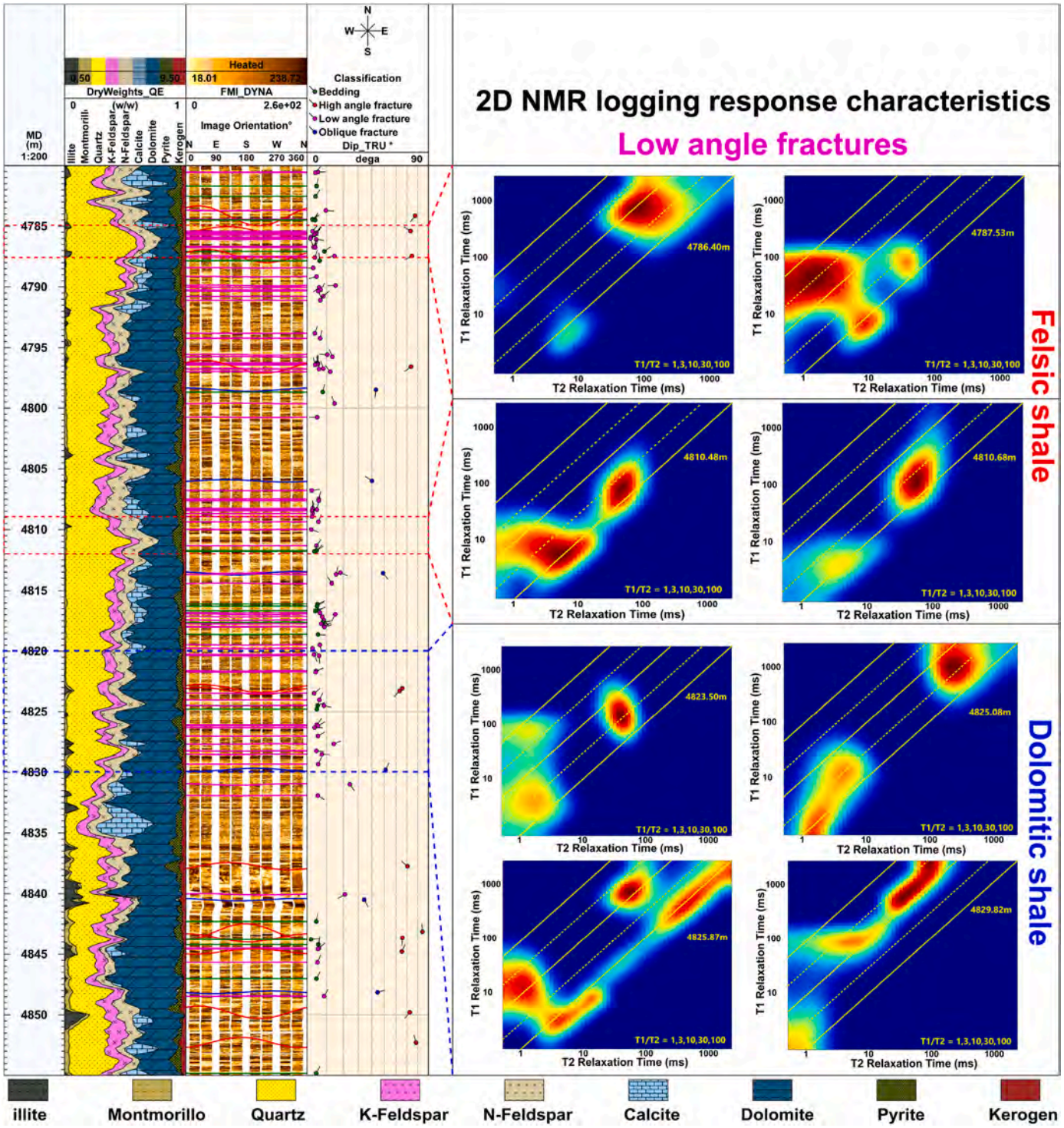

Fig. 18. The relationship between reservoir quality and natural fractures in the lithofacies assemblage unit of interbedded felsic shale and dolomitic shale.

shale sections. Bedding planes serve as stress-weakening surfaces, making the rocks more susceptible to fracturing along lamination and foliation under stress, thereby forming low-angle fractures and horizontal fractures. Intergranular pores associated with felsic minerals and intercrystalline pores related to dolomite provide reservoir spaces within the shale. Coupled with the development of low-angle fractures, these intervals can also serve as targets for hydraulic fracturing to enhance production.

6. Conclusion

The shale of the Fengcheng Formation in the Mahu Sag is a typical set of continental shales with laminar and bedding features formed in a lacustrine depositional environment. Influenced by seasonal variations, climate, provenance, volcanic activity, and water temperature, the reservoir exhibits strong heterogeneity characterized by mixed mineral compositions, vertically stacked thin interlayers, and well-developed laminae and bedding. During subsequent diagenesis and burial processes, the shale underwent multiple phases of stress-induced

modification, resulting in observable multi-scale natural fractures. According to the occurrence of these natural fractures, individual fractures can be classified into three types: high-angle fractures, oblique fractures, and low-angle fractures.

Shear wave data extracted from acoustic logging, especially radial fast and slow shear waves and far-detection reflected shear waves, show significant responses to natural fractures and reflectors. These unique response characteristics can be utilized to identify natural fractures. In sections where fractures are developed, both fast and slow shear waves along the radial direction exhibit a pattern of increasing followed by decreasing amplitudes, with the occurrence of intersection points in acoustic time differences. After data processing methods such as filtering, migration, and stacking, shear wave reflections can present images similar to seismic profiles. Far-detection shear wave reflection profiles can reveal reflectors (fractures) at a distance from the borehole wall. By integrating imaging logging, radial profiles of fast and slow shear waves, and multi-azimuth far-detection reflection wave profiles for specialized fracture identification, the ambiguity in fracture recognition can be effectively reduced.

Elemental logging (Lithoscanner) is employed to clarify the mineral composition characteristics of the shale reservoir, while two-dimensional nuclear magnetic resonance (CMR-NG) logging is used to elucidate pore structure and oil-bearing features. Combined with the methods presented in this paper to summarize the vertical distribution characteristics of natural fractures, the relationships among mineral composition, natural fractures, and reservoir quality are clarified. The study indicates that the development of interlayers between felsic shale and mudstone tends to form high-angle fractures and network fractures. When laminated dolomitic shale and felsic shale interlayers are present, low-angle fractures and horizontal fractures are more likely to form. An increase in clay mineral content leads to deterioration of the reservoir's pore structure and brittleness, an increase in bound water content within reservoir fluids, and overall poor reservoir quality. Conversely, higher contents of felsic minerals and dolomite improve the reservoir's pore structure and enhance brittleness, resulting in lower bound water content, higher movable oil content, and better reservoir quality. Therefore, during fracturing and perforation operations, intervals with relatively high contents of felsic minerals and dolomite should be selected to achieve greater productivity.

CRediT authorship contribution statement

Song Wang: Writing – review & editing, Writing – original draft. **Guiwen Wang:** Project administration, Methodology. **Lianbo Zeng:** Methodology. **Peng Liu:** Formal analysis, Data curation. **Yuyue Huang:** Supervision, Software, Investigation. **Shiqian Li:** Visualization, Investigation. **Zhishi Wang:** Software, Data curation. **Yuanlong Zhou:** Funding acquisition, Investigation.

Declaration of competing interest

The authors declare that they have no known competing financial interests or personal relationships that could have appeared to influence the work reported in this paper.

Acknowledgements

This work is financially supported by the China Postdoctoral Science Foundation (2024M753612 and GZC20233101) and National Key R&D Program of China (2022YFE0206800). Also Supported by Science Foundation of China University of Petroleum, Beijing (No. 2462023XKBH012). In addition, the authors would like to express their sincere thanks to the PetroChina Xinjiang Oilfield Company for their assistance in providing the information and for their technical input to this work.

Data availability

The authors do not have permission to share data.

References

Anders, M.H., Laubach, S.E., Scholz, C.H., 2014. Microfractures: a review. J. Struct. Geol. 69, 377–394.
Brekke, H., Roenitz, T., 2021. Using high-resolution microresistivity image logs to reconstruct paleoenvironments and stratal architectures: an example from the mcmurray formation, leismer area, northeastern alberta, Canada. Aapg Bull. 105, 1563–1593.
Cai, C., Wang, L., Zhang, R., Kang, Q., Zhang, Q., Zhao, D., Guo, J., Chen, M., Chen, H., Lei, L., Wang, K., He, J., 2024. Two-dimensional spectrum characteristics and oil movability study of the shale oil reservoir. Front. Energy Res. 12, 1389877.
Cao, J., Zhang, Y.J., Hu, W.X., Yao, S.P., Wang, X.L., Zhang, Y.Q., Tang, Y., 2005. The permian hybrid petroleum system in the northwest margin of the junggar basin , northwest China. Mar. Petrol. Geol. 22, 331–349.
Chen, D., Zhang, C., Guan, W., Wang, J., 2023. Near-borehole formation acoustic logging imaging: a full waveform inversion algorithm in cylindrical coordinates. Ieee T. Geosci. Remote 61, 3312270.
Dai, Q., Wang, G., Zhao, X., Han, Z., Lu, K., Lai, J., Wang, S., Li, D., Li, Y., Wu, K., 2021. Fractal model for permeability estimation in low-permeable porous media with variable pore sizes and unevenly adsorbed water lay. Mar. Petrol. Geol. 130, 105135.
Du, X., Jin, Z., Zeng, L., Liu, G., He, W., Ostadhassan, M., Liang, X., Yang, S., Lu, G., 2023. Characteristics and controlling factors of natural fractures in deep lacustrine shale oil reservoirs of the permian fengcheng formation in the mahu sag, junggar basin, China. J. Struct. Geol. 175, 104923.
Eyinla, D., Henderson, S.K., Emadi, H., Raj Thiyagarajan, S., Arora, A., 2023. Optimization of hydraulic fracture monitoring approach: a perspective on integrated fiber optics and sonic tools. Geoenergy Science and Engineering 231, 212441.
Fleury, M., Romero-Sarmiento, M., 2016. Characterization of shales using t 1 - t 2 nmr maps. J. Petrol. Sci. Eng. 137, 55–62.
Fu, X., Gou, Y., Wei, F., 2024. Acoustic logging array signal denoising using u-net and a case study in a tanggu oil field. J. Geophys. Eng. 21, 981–992.
Guo, P., Wen, H., Gibert, L., Jin, J., Wang, J., Lei, H., 2021. Deposition and diagenesis of the early permian volcanic-related alkaline playa-lake dolomitic shales , nw junggar basin, nw China. Mar. Petrol. Geol. 123, 104780.
Guo, T., Rui, Z., Qu, Z., Qi, N., 2018. Experimental study of directional propagation of hydraulic fracture guided by multi-radial slim holes. J. Petrol. Sci. Eng. 166, 592–601.
He, X., Luo, Q., Jiang, Z., Qiu, Z., Luo, J., Li, Y., Deng, Y., 2024. Control of complex lithofacies on the shale oil potential in saline lacustrine basins of the jimsar sag, nw China: coupling mechanisms and conceptual models. J. Asian Earth Sci. 266, 106135.
Hu, T., Pang, X., Yu, S., Wang, X., Pang, H., Guo, J., Jiang, F., Shen, W., Wang, Q., Xu, J., 2016. Hydrocarbon generation and expulsion characteristics of lower permian p 1 f source rocks in the fengcheng area, northwest margin, junggar basin, nw China: implications for tight oil accumulation potential assessment. Geol. J. 51, 880–900.
Huang, Y., Wang, G., Zhang, Y., Xi, J., Huang, L., Wang, S., Zhang, Y., Lai, J., Jiang, C., 2023. Logging evaluation of pore structure and reservoir quality in shale oil reservoir: the fengcheng formation in mahu sag , junggar basin, China. Mar. Petrol. Geol. 156, 106454.
Ju, W., Niu, X., Feng, S., You, Y., Xu, K., Wang, G., Xu, H., 2020. Predicting the present-day in situ stress distribution within the yanchang formation chang 7 shale oil reservoir of ordos basin, central China. Pet. Sci. 17, 912–924.
Kausik, R., Fellah, K., Rylander, E., Singer, P.M., Sinclair, S.M., 2016. NMR relaxometry in shale and implications for logging. Petrophysics 57 (4), 339.
Kamel, M.H., Mabrouk, W.M., 2004. Estimating seismic impedance and elastic parameters in hydrocarbon-bearing reservoirs from acoustic logs. J. Petrol. Sci. Eng. 45, 21–29.
Khoshbakht, F., Azizzadeh, M., Memarian, H., Nourozi, G.H., Moallemi, S.A., 2012. Comparison of electrical image log with core in a fractured carbonate reservoir. J. Petrol. Sci. Eng. 86–87, 289–296.
Lai, J., Su, Y., Xiao, L., Zhao, F., Bai, T., Li, Y., Li, H., Huang, Y., Wang, G., Qin, Z., 2024. Application of geophysical well logs in solving geologic issues: past, present and future prospect. Geosci. Front. 15, 101779.
Li, D., 2023. A three-dimensional display technology of reflected acoustic logging and its application example. Geofluids 2023, 7979348.
Li, H., Tang, X., Li, S., Su, Y., 2022. Dynamic fluid transport property of hydraulic fractures and its evaluation using acoustic logging. Petrol. Explor. Dev. 49, 223–232.
Liu, G., Chen, Z., Wang, X., Gao, G., Xiang, B., Ren, J., Ma, W., 2016. Migration and accumulation of crude oils from permian lacustrine source rocks to triassic reservoirs in the mahu depression of junggar basin, nw China: constraints from pyrrolic nitrogen compounds and fluid inclusion analysis. Org. Geochem. 101, 82–98.
Ma, T., Gui, J., Chen, P., 2021. Logging evaluation on mechanical-damage characteristics of the vicinity of the wellbore in tight reservoirs. J. Pet. Explor. Prod. Technol. 11, 3213–3224.
Ma, X., Wang, H., Zhou, S., Feng, Z., Liu, H., Guo, W., 2020. Insights into nmr response characteristics of shales and its application in shale gas reservoir evaluation. J. Nat. Gas Sci. Eng. 84, 103674.
Mazdarani, A., Kadkhodaie, A., Wood, D.A., Soluki, Z., 2023. Natural fractures characterization by integration of fmi logs, well logs and core data: a case study from the sarvak formation (Iran). J. Pet. Explor. Prod. Technol. 13, 1247–1263.

Nian, T., Wang, G., Tan, C., Fei, L., He, W., Wang, S., 2021. Hydraulic apertures of barren fractures in tight-gas sandstones at depth: image-core calibration in the lower cretaceous bashijiqike formation , tarim basin. J. Petrol. Sci. Eng. 196, 108016.
Sun, L., Cui, B., Zhu, R., Wang, R., Feng, Z., Li, B., Zhang, J., Gao, B., Wang, Q., Zeng, H., Liao, Y., Jiang, H., 2023. Shale oil enrichment evaluation and production law in gulong sag, songliao basin, ne China. Petrol. Explor. Dev. 50, 505–519.
Tan, P., Pang, H., Zhang, R., Jin, Y., Zhou, Y., Kao, J., Fan, M., 2020. Experimental investigation into hydraulic fracture geometry and proppant migration characteristics for southeastern sichuan deep shale reservoirs. J. Petrol. Sci. Eng. 184, 106517.
Tang, W., Song, Y., He, W., Tang, Y., Guo, X., Pe-Piper, G., Piper, D.J.W., Li, W., Guo, Z., Zhang, Y., 2022. Source-to-sink evolution of syn-rift alkaline lake sediments in the lower permian fengcheng formation, junggar basin , nw China: evidence from petrology, detrital zircon geochronology and geochemistry. J. Asian Earth Sci. 232, 105049.
Tang, W., Zhang, Y., Pe-Piper, G., Piper, D.J.W., Guo, Z., Li, W., 2021. Soft-sediment deformation structures in alkaline lake deposits of lower permian fengcheng formation , junggar basin, nw China: implications for syn-sedimentary tectonic activity. Sediment. Geol. 422, 105719.
Trichandi, R., Bauer, K., Ryberg, T., Wawerzinek, B., Vargas, J.A., von Blanckenburg, F., Krawczyk, C.M., 2023. Shear-wave velocity imaging of weathered granite in la campana (chile) from bayesian inversion of micro-tremor h/v spectral ratios. J. Appl. Geophys. 217, 105191.
Wang, H., Li, N., Wang, C., Wu, H., Liu, P., Li, Y., Liu, Y., 2020. Responses of dipole-source reflected shear waves in acoustically slow formations. J. Geophys. Eng. 17, 1–17.
Wang, L., Lyu, Q., Li, L., Liu, J., Luo, S., Sun, X., Zhang, L., Xu, X., 2024a. Sedimentary characteristics of mixed source fi ne-grained gravity- fl ow and its signi fi cance for shale oil exploration in a lacustrine depression basin: a case study of the chang 7 3 sub-member of the triassic yanchang formation in ordos basin, nw China. Sediment. Geol. 464, 106629.
Wang, S., Wang, G., Huang, L., Song, L., Zhang, Y., Li, D., Huang, Y., 2021. Logging evaluation of lamina structure and reservoir quality in shale oil reservoir of fengcheng formation in mahu sag. china. Mar. Petrol. Geol. 133, 105299.
Wang, X., Jin, Z., Chen, G., Peng, M., Huang, L., Wang, Z., Zeng, L., Lu, G., Du, X., Liu, G., 2022. Multi-scale natural fracture prediction in continental shale oil reservoirs: a case study of the fengcheng formation in the mahu sag, junggar basin, China. Front. Earth Sci. 10, 929467.
Wang, Y., Zhai, C., Liu, T., Yu, X., Xu, J., Sun, Y., Cong, Y., Tang, W., Zheng, Y., Luo, N., 2024b. Analysis of fracture network formation mechanisms and main controlling factors of methane explosion fracturing in deep shale reservoir. Rock Mech. Rock Eng. 57, 7125–7147.
Wu, H., Wang, C., Feng, Z., Yuan, Y., Wang, H., Xu, B., 2020. Adaptive multi-resolution graph-based clustering algorithm for electrofacies analysis. Appl. Geophys. 17, 13–25.
Wu, X., Wang, F., Zhang, X., Han, B., Liu, Q., Zhang, Y., 2024. Extraction of fractures in shale ct images using improved u-net. Energy Geoscience 5, 100185.
Xi, K.L., Li, K., Cao, Y.C., Lin, M.R., Niu, X.B., Zhu, R.K., Wei, X.Z., You, Y., Liang, X.W., Feng, S.B., 2020. Laminae combination and shale oil enrichment patterns of chang 7 3 sub-member organic-rich shales in the triassic yanchang formation , ordos basin, nw China. Petrol. Explor. Dev. 47, 1342–1353.
Xiao, F., Yang, J., Li, S., Yao, Y., Huang, Y., Gao, X., 2024. Enrichment and movability of lacustrine tight shale oil for the first member of the upper cretaceous qingshankou formation in the sanzhao sag, songliao basin, ne China: insights from saturated hydrocarbon molecules. Fuel 368, 131615.
Xu, H., Zhai, C., Sun, Y., Xia, J., Lai, Y., Dong, X., Xu, H., Huang, T., Cai, Y., 2024. Imaging small geological structure in coal mines based on reflected acoustic logging of underground cross-seam boreholes. Geoenergy Science and Engineering 234, 212675.
Yang, Z., Wang, X., Ge, H., Zhu, J., Wen, Y., 2022. Study on evaluation method of fracture forming ability of shale oil reservoirs in fengcheng formation, mahu sag. J. Petrol. Sci. Eng. 215, 110576.
Yu, K., Cao, Y., Qiu, L., Sun, P., 2018. The hydrocarbon generation potential and migration in an alkaline evaporite basin: the early permian fengcheng formation in the junggar basin , northwestern China. Mar. Petrol. Geol. 98, 12–32.
Yu, K., Zhang, Z., Cao, Y., Qiu, L., Zhou, C., Cheng, D., Sun, P., Yang, Y., 2021. Origin of biogenic-induced cherts from permian alkaline saline lake deposits in the nw junggar basin , nw China: implications for hydrocarbon exploration. J. Asian Earth Sci. 211, 104712.
Zhang, C., Chen, D., Hu, H., Wang, J., He, X., 2024. A method for transforming aliased modes to true modes based on density clustering and riemann sheets selection in acoustic logging dispersion inversion. Geophysics 89, D15–D29.
Zhang, Q., Zhang, X., Sun, W., 2021. A review of laboratory studies and theoretical analysis for the interaction mode between induced hydraulic fractures and pre-existing fractures. J. Nat. Gas Sci. Eng. 86, 103719.
Zhang, Z.J., Yuan, X.J., Wang, M.S., Zhou, C.M., Tang, Y., Chen, X.Y., Lin, M.J., Cheng, D.W., 2018. Alkaline-lacustrine deposition and paleoenvironmental evolution in permian fengcheng formation at the mahu sag, junggar basin , nw China. Petrol. Explor. Dev. 45, 1036–1049.
Zhao, W.Z., Hu, S.Y., Hou, L.H., Yang, T., Li, X., Guo, B.C., Yang, Z., 2020. Types and resource potential of continental shale oil in China and its boundary with tight oil. Petrol. Explor. Dev. 47, 1–11.
Zhi, D., Tang, Y., He, W., Guo, X., Zheng, M., Huang, L., 2021. Orderly coexistence and accumulation models of conventional and unconventional hydrocarbons in lower permian fengcheng formation, mahu sag, junggar basin. Petrol. Explor. Dev. 48, 43–59.
Zhu, L., Zhang, C., Guo, C., Jiao, Y., Chen, L., Zhou, X., Zhang, C., Zhang, Z., 2018. Calculating the total porosity of shale reservoirs by combining conventional logging and elemental logging to eliminate the effects of gas saturation. Petrophysics 59, 162–184.
Zhuang, C., Xu, S., Li, H., Su, Y., Tang, X., 2019. Azimuthal shear-wave anisotropy measurement in a borehole: physical modeling and dipole acoustic verification. J. Acoust. Soc. Am. 146, 129–134.
Zou, C., Yang, Z., Li, G., Li, J., Liu, X., Tang, Y., Jiang, T., Yang, Y., Bai, X., Pan, S., Lu, M., Lei, Z., Cai, B., 2022. Why can China realize the continental " shale oil revolution"? J. Earth Sci. 33, 1324–1327. China.